TECTONIC SIGNIFICANCE OF THE CUMULATE GABBROS WITHIN KULUNCAK OPHIOLITIC SUITE (MALATYA, SE TURKEY) INFERRED FROM GEOCHEMICAL DATA

Murat Camuzcuoğlu*, **Utku Bağcı***,✉, **Jürgen Koepke**** and **Paul Eric Wolff****

* *Mühendislik Fakültesi Jeoloji Mühendisliği Bölümü, Mersin Üniversitesi, Türkiye.*
** *Institut für Mineralogie, Universität Hannover, Germany.*
✉ *Corresponding author, email: bagciutku@gmail.com*

Keywords: *ophiolite, cumulate, suprasubduction zone, mineral chemistry, Inner Tauride. Turkey.*

ABSTRACT

The Kuluncak (Malatya) ophiolite in the Eastern Tauride, Turkey, consists of mantle tectonites, ultramafic-mafic cumulates, isotropic gabbros, a sheeted dike complex, plagiogranites, and a volcanic complex. The best exposure of the mafic cumulate rocks of the Kuluncak ophiolite is in the Hekimhan region, where they are represented by olivine gabbro and gabbro showing orthocumulate to mesocumulate textures. The cumulus and postcumulus minerals do not show significant zoning. The crystallization order of the cumulates is olivine, plagioclase, clinopyroxene and orthopyroxene. Whole-rock major- and trace-element geochemistry of the mafic cumulate rocks indicates that the primary magma generating the Kuluncak ophiolite is similar in composition to those observed in modern island-arc tectonic settings. Rare earth element (REE) concentrations of the mafic cumulates exhibit depleted light rare earth element (LREE) patterns, with Ce_N/Sm_N and Ce_N/Yb_N ratios ranging from 0.21 to 0.75 and from 0.17 to 0.66, respectively. The coexistence of anorthite-rich plagioclase ($An_{73.4-93.7}$), highly magnesian olivine ($Fo_{65.2-86.9}$), clinopyroxene ($Mg\#_{75-92.1}$), and orthopyroxene ($Mg\#_{77.6-84.3}$) in the cumulate gabbroic rocks is indicative of an intra-oceanic subduction setting and suggests that the Kuluncak ophiolite was formed during the Late Cretaceous closure of the Inner Tauride Ocean.

INTRODUCTION

Over the past three decades, petrologic and geochemical studies of cumulate rocks have played a significant role in clarifying their petrogenesis and the magma chamber processes (Juteau and Whitechurch, 1980; Thy, 1987; 1990; Hébert and Laurent, 1990; Parlak et al., 1996; 2000; 2002; Bağcı et al., 2005; 2006; İlbeyli, 2008; Sarıfakıoğlu et al., 2009; Bağcı, 2013; Parlak et al., 2013). Furthermore, the relationship between cumulate rock composition and an island-arc tectonic setting have been proposed for the Eastern Mediterranean ophiolites (Burns, 1985; DeBari et al., 1987; DeBari and Coleman, 1989; Spandler et al., 2003).

Late Cretaceous ophiolites in Turkey crop out in five suture zones: the Pontide, Anatolian, Tauride, SE Anatolian, and peri-Arabian ophiolites (Fig. 1) (Robertson, 2002). The well-documented Neotethyan ophiolites of Turkey show a suprasubduction zone (SSZ) geochemical signature (Yalınız et al., 1996; Parlak et al., 1996; 2000; 2002; 2004; 2009; 2013; Beyarslan and Bingöl, 2000; Robertson, 2002; Robertson et al., 2006; 2007; Bağcı et al., 2005; 2006; 2008; Rızaoğlu et al., 2006; Bağcı and Parlak, 2009; Dilek and Thy, 2009). However, only limited petrologic and geochemical data (Camuzcuoğlu, 2012; Metin et al., 2013) are available for ophiolitic rocks from the area between Hekimhan and Kuluncak, which is northwest of Malatya, in the Tauride belt (Figs. 1, 2). In this paper, we focus on the mafic cumulate rocks of the Kuluncak (Malatya) ophiolite. The aims of this study are (1) to provide whole-rock and mineral chemistry of mafic cumulate rocks, (2) to compare the obtained results with data on the eastern Mediterranean ophiolites and (3) to emphasize the occurrence of cumulate rocks and their tectonic significance.

REGIONAL GEOLOGY

The Kuluncak-Hekimhan-Hasançelebi region (Fig. 2) is in the Eastern Tauride system and consists of Jurassic-Cretaceous neritic limestones, Late Cretaceous ophiolitic rocks, and latest Cretaceous-Late Eocene sedimentary and igneous rocks of the Hekimhan Basin (Gürer, 1992; 1994; Metin et al., 2013; Booth et al., 2014). The stratigraphically oldest unit is composed of carbonate platform rocks, locally named Geniz Formation (Booth et al., 2014). This formation is tectonically overlain by Late Cretaceous ophiolitic rocks. The Hekimhan Formation, which unconformably overlies the ophiolitic rocks, contains carbonate and clastic rocks and represents marine transgression within the Hekimhan Basin (Gürer, 1994; Booth et al., 2014). The Maastrichtian sedimentation was contemporaneous with the formation of volcanogenic rocks, known as the Hasançelebi Formation, which includes (extrusive and intrusive) rocks and associated clastic sediments. The extrusive volcanic rocks consist of basaltic pillow lavas, lava flows and volcanic breccias. The intrusive basaltic dykes cut the Hasançelebi Formation lavas and the Hekimhan Formation sediments. The alkaline Yüceşafak syenite consists mainly of syenite and quartz syenite, with minor monzonite or quartz monzonite, which have been chemically modified by metasomatic, hydrothermal, or weathering processes. Isolated syenitic dykes cut the basaltic rocks of the Hasançelebi Formation. The Akpınar Formation, which overlies Maastrichtian limestones, consists primarily of sedimentary rocks of Paleocene-Eocene age (Gürer, 1992; Metin et al., 2013; Booth et al., 2014). Oligocene clastics (Kamatlar Formation) unconformably overlie the Akpınar Formation and consist mainly of red fluvial sandstones and conglomerates. The Kamatlar Formation is unconformably overlain by Miocene limestones (Boyralı Formation). This unit is overlain by Late Miocene-Pliocene volcanic rocks (Yamadağ volcanics), which consist of pyroclastics, andesites and basalts (Yalçın et al., 1998). The contact between the surficial Quaternary alluvium and the underlying units is an angular unconformity.

Dismembered Neotethyan ophiolitic rocks crop out between Hekimhan and Kuluncak approximately 80 km

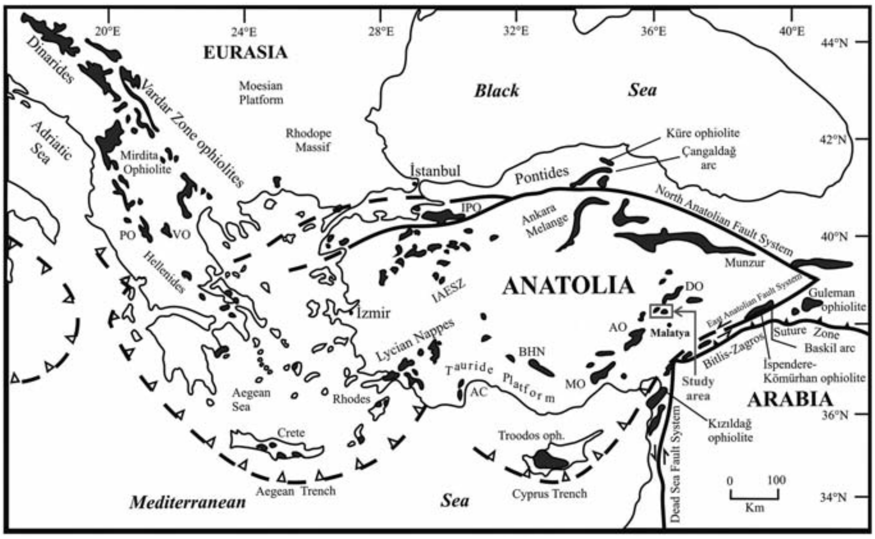

Fig. 1 - Distribution of the Neotethyan ophiolites and major tectonic features in Eastern Mediterranean region (from Dilek and Flower, 2003). AC- Antalya Complex; IPO- Intra Pontide Ophiolites; BHN- Beyşehir-Hoyran Nappes; İAESZ- İzmir-Ankara-Erzincan Suture Zone; MO- Mersin Ophiolite; PO- Pindos Ophiolite; VO- Vourinous Ophiolite; AO- Aladağ Ophiolite; DO- Divriği Ophiolite.

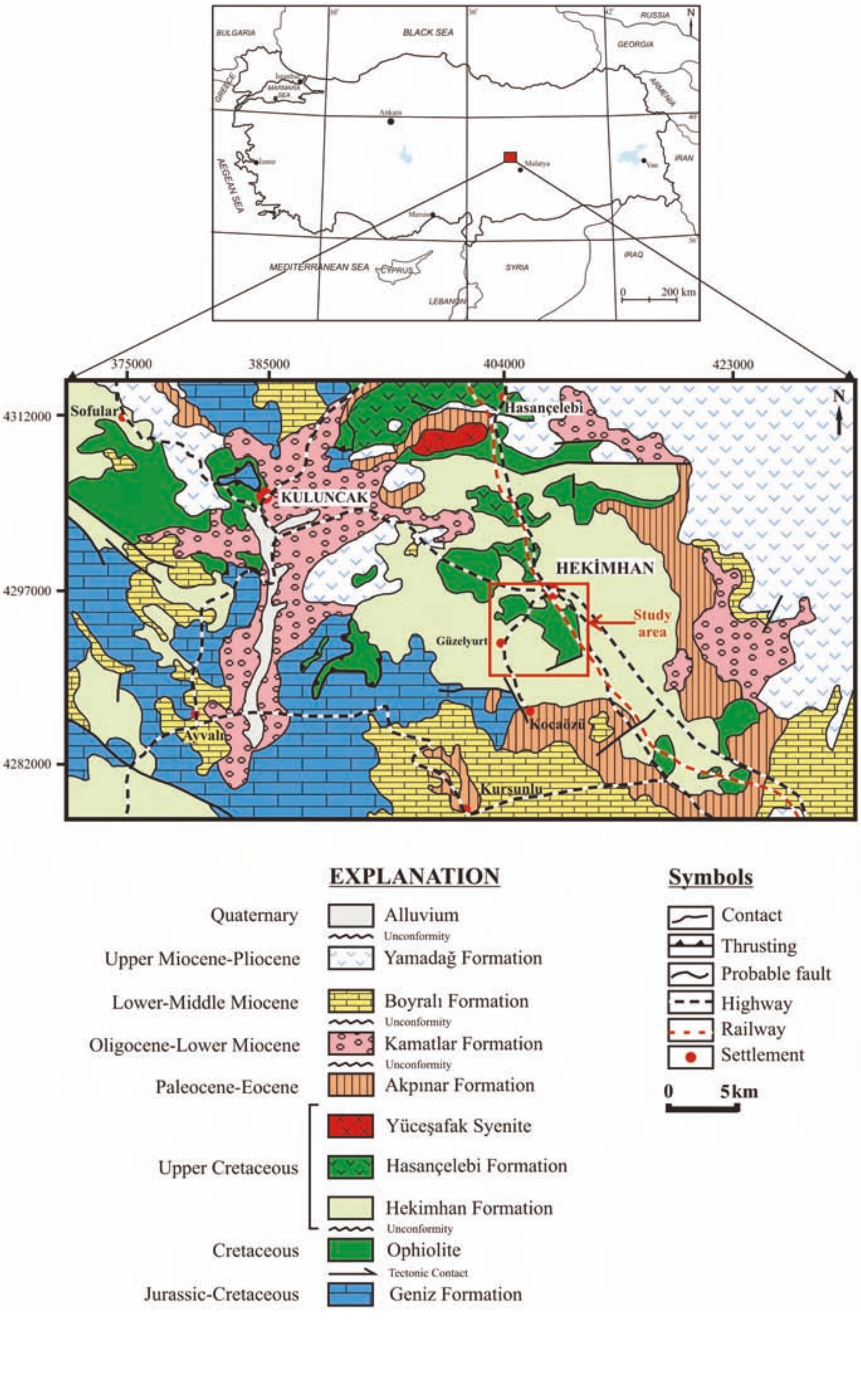

Fig. 2 - Simplified geological map of the Kuluncak-Hekimhan region (modified from the 1:500.000 Geological map of Turkey, Sivas sheet, MTA, 2002). The location of Fig. 4 is indicated as "Study area".

northwest of the city of Malatya in the Eastern Tauride Mountains (Fig. 2). The ophiolitic rocks, locally called the Hocalıkova ophiolites (Gürer, 1992; 1994), represent a disrupted and incomplete ophiolite sequence. The ophiolites are extensively exposed in the area under investigation (Fig. 2), whereas the Mesozoic Tauride carbonate platform is exposed to the west. Approximately 70 km farther west, small outcrops of dismembered ophiolites are exposed along the southwestern margin of the Darende Basin. The dismembered ophiolites, renamed the Kuluncak ophiolite, can be restored as a complete ophiolite sequence consisting of the following rocks, from the bottom to the top: mantle tectonites, ultramafic-mafic cumulates, isotropic gabbros, a sheeted dike complex, plagiogranites and a volcanic complex (Fig. 3) (Yılmaz et al., 2005; Rızaoğlu et al., 2010; Camuzcuoğlu, 2012; Camuzcuoğlu et al., 2013; Metin et al., 2013). The contact relations between the subunits of the ophiolite are mainly tectonic. The mantle tectonites, cumulates and isotropic gabbros are intruded by isolated dikes.

In the study area, the mantle tectonites are well exposed at Kösrelik, Karatepe and Ataçoğluevsünü (Figs. 4, 5a) and consist of dunites, harzburgites, serpentinites and chromitites. Locally, rodingite veins and dykes cut across the peridotites and serpentinites (Fig. 5b). The rodingites are mainly composed of hydrogarnet, clinozoisite, wollastonite, amphibole, plagioclase, chlorite and titanite (Camuzcuoğlu and Bağcı, 2016). The ultramafic-mafic cumulate rocks display igneous layering, cross-bedding, graded bedding and other cumulate structures (Fig. 5c-e). The ultramafic cumulates are dominated by dunites, wehrlites and pyroxenites, whereas the gabbroic cumulates are represented by low-Ti olivine-gabbros and gabbros. The mafic cumulate rocks in the Kuluncak ophiolite crop out mainly along Pamuklu Tepe to the

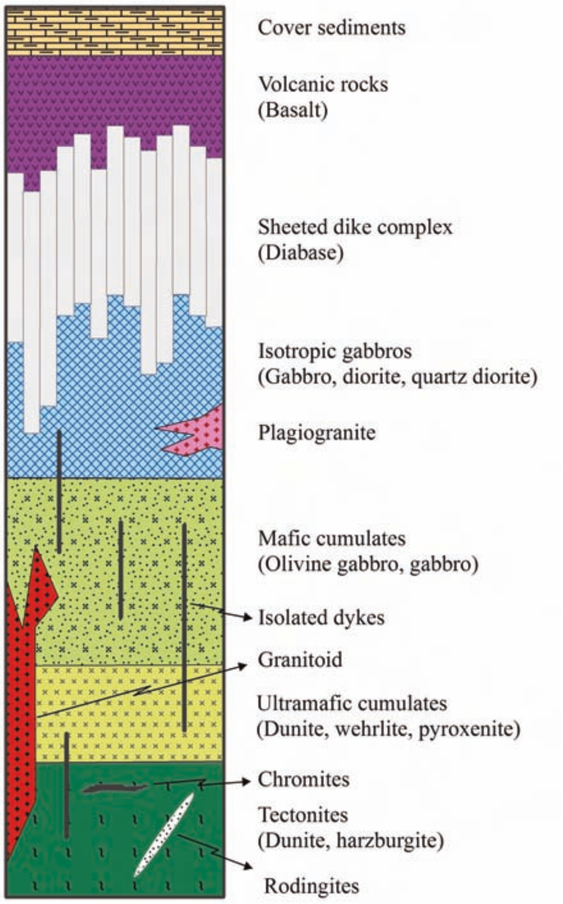

Fig. 3 -Synthetic log of Kuluncak (Malatya) ophiolite (Rızaoğlu et al., 2010; Metin et al., 2013).

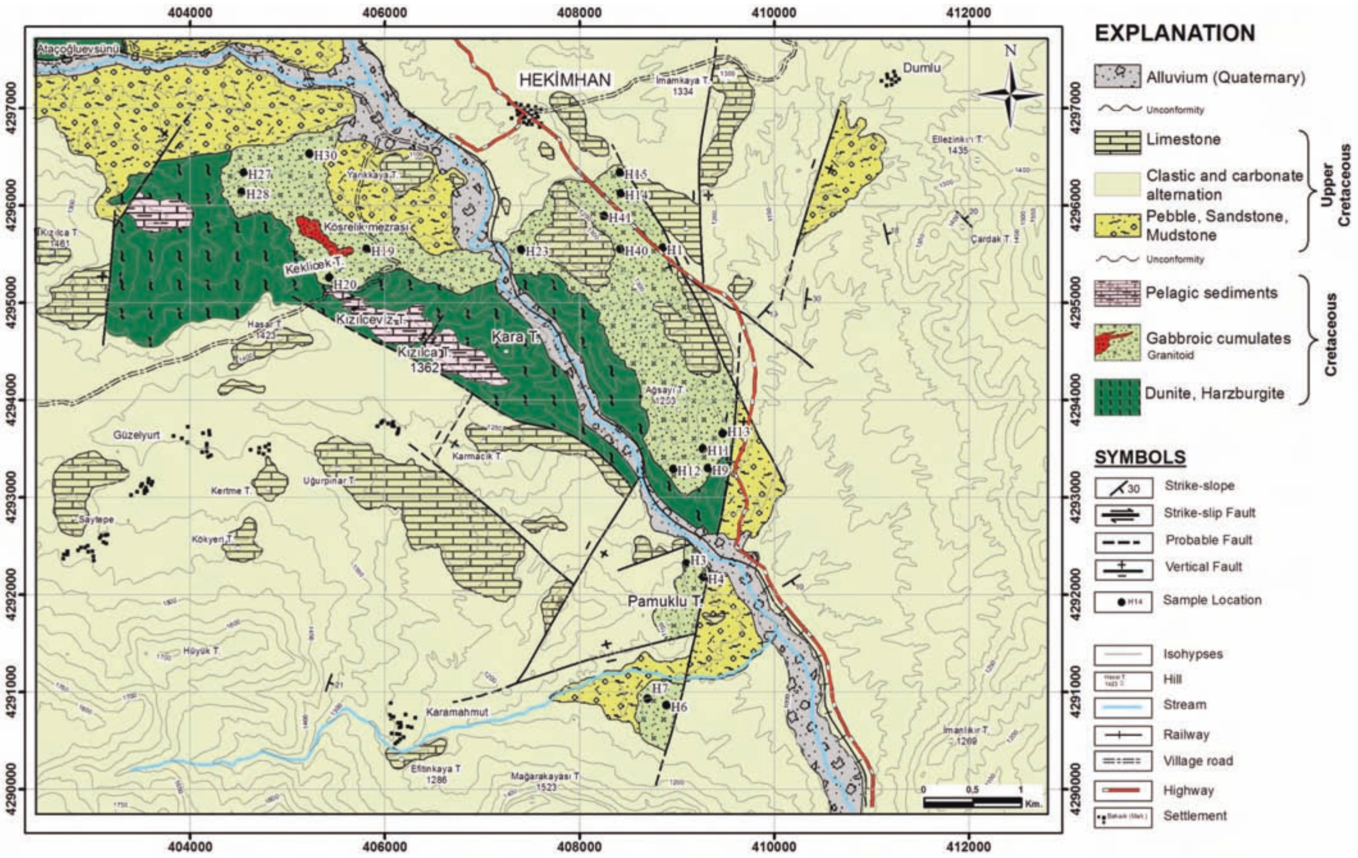

Fig. 4 - Geological map of the southern Hekimhan region (Camuzcuoğlu, 2012).

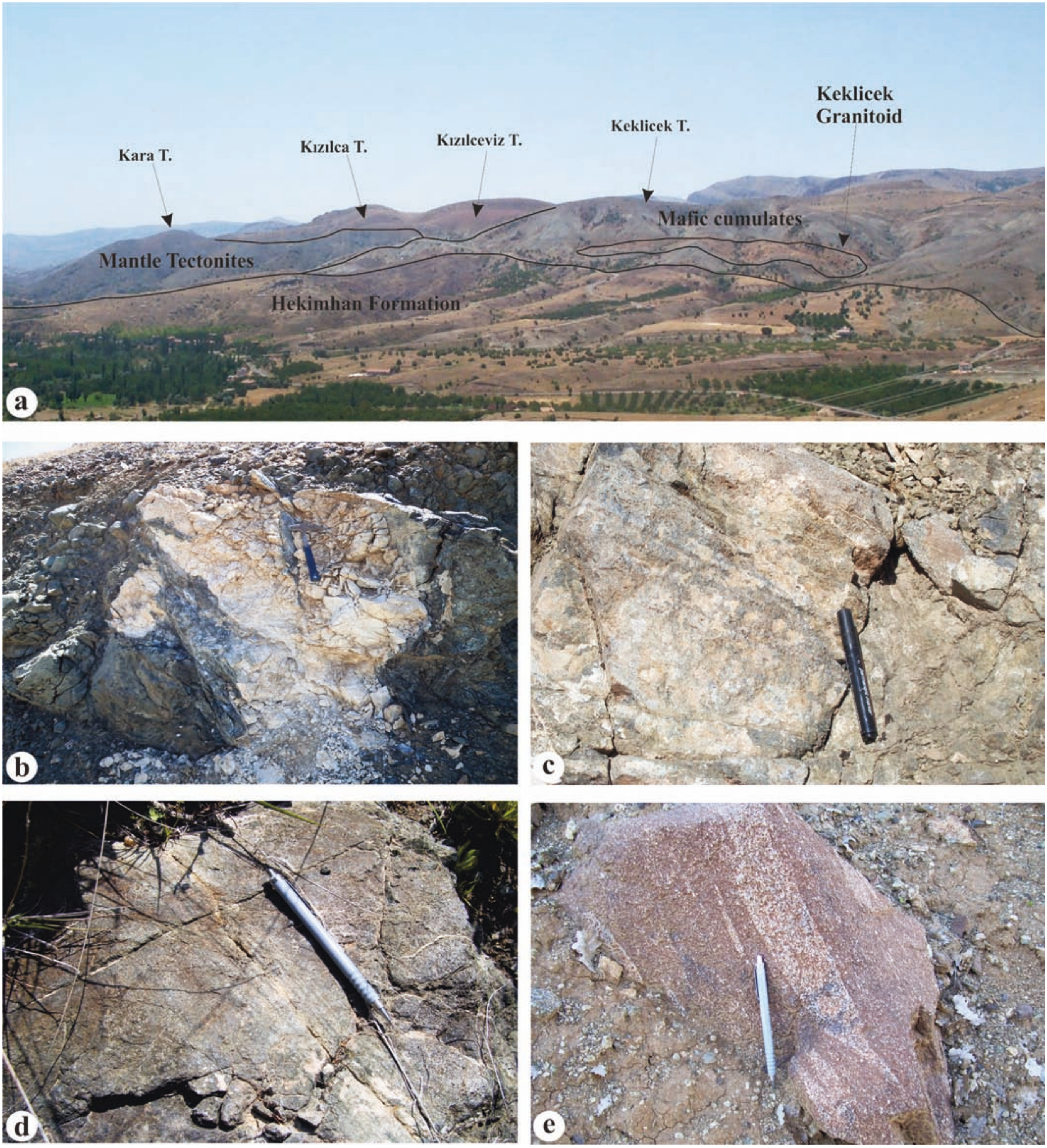

Fig. 5 - (a) Field relations and rocks units of the Kuluncak ophiolite; (b) rodingitized dyke (white) in serpentinized peridotite; (c, d) igneous layering and lamination (e) cross bedding in the mafic cumulate rocks.

southeast and Keklicek Tepe to the northwest. The isotropic gabbros are gabbroic and dioritic or quartz dioritic in composition and have granular to ophitic or subophitic textures. The sheeted dike complex is composed of diabasic dykes (Yılmaz et al., 2005), whereas the isolated dykes are made up of dolerite and microdiorite with ophitic, intersertal and microgranular textures (Rızaoğlu et al., 2010). The volcanic complex consists mainly of pillow basalts covered by radiolarites, cherts, pelagic limestones and hemipelagic mudstones (Rızaoğlu et al., 2010; Metin et al., 2013). Brown- and red- to pink-colored pelagic limestones are observed on Kızılceviz Tepe and Kızılca Tepe. The Keklicek granitoid intrudes cumulate rocks at Keklicek Tepe in the study area. The Kuluncak ophiolitic sequences are unconformably overlain by Maastrichtian post-emplacement reddish-brown clastic sediments, pertaining to the Karadere Formation and the transgressive Hekimhan Formation, which consists of alternating clastics and carbonates.

SAMPLING AND ANALYTICAL METHODS

For petrographic and chemical analyses, samples were collected around the village of Hekimhan and to the south of the Hasançelebi from outcrops of the mafic cumulates within the Kuluncak (Malatya) ophiolite (Figs. 2, 3). A total of 25 selected samples (15 olivine gabbros and 10 gabbros) were analyzed for major and trace elements at ACME Analytical Laboratories in Vancouver, Canada. After $LiBO_2$ fusion and nitric-acid digestion of the rock powders, major-element, trace-element, and REE analyses were performed on the solutions by inductively coupled plasma-atomic emission spectrometry (ICP-AES). Loss on ignition (LOI) was calculated as the weight difference after ignition at 1000°C. Detection limits range from 0.002 to 0.04 wt% for major oxides, 0.1 to 8 ppm for trace elements and 0.05 to 0.1 ppm for REEs.

Microprobe analyses were performed on approximately 480 points in 6 representative polished thin sections from the mafic cumulates of the Kuluncak ophiolite. Mineral compositions were determined using a CAMECA SX-100 electron microprobe at the Institute of Mineralogy in Hannover, Germany. The analytical conditions were 15kV for the acceleration voltage, 15nA for the beam current and 10 to 30 secs of counting time for silicates. Raw data were revised by a PAP (Pouchou and Pichoir, 1984) matrix correction. The microprobe detection limits in weight percent for the oxides are 0.09 for Si, Mg; 0.07 for Al, Ca and Na; 0.13 for Fe and Mn; 0.04 for Ti; 0.08 for Cr; 0.02 for K; and 0.10 for Ni.

PETROGRAPHY AND MINERAL CHEMISTRY

The mafic cumulates of the Kuluncak (Malatya) ophiolite are composed of olivine gabbros and gabbros characterized by orthocumulate and mesocumulate texture (cf. Wager et al., 1960) with cumulus and intercumulus olivine, clinopyroxene and plagioclase. The olivine gabbros (Fig. 6a) consist mainly of 40-55 vol% plagioclase with a grain size of 0.05-0.75 mm, 21-43 vol% clinopyroxene with a grain size of 0.05-0.9 mm, 10-25 vol% olivine with a grain size of 0.05-1.25 mm and 2 vol% intercumulus anhedral orthopyroxene with a grain size of 0.02-0.15 mm, 2 vol% intercumulus amphibole (Fig. 6b) with a grain size of approximately 0.02 mm. The gabbros (Fig. 6c) are made of 43-64 vol% plagioclase with a grain size of 0.05-0.8 mm, 32-51 vol% clinopyroxene with a grain size of 0.05-0.5 mm and 5-8 vol% olivine with a grain size of 0.05-0.4 mm. Clinopyroxene is partly or completely altered to green-brown amphibole in gabbroic samples (Fig. 6d). The serpentine, fibrous actinolite, sericite, kaolinite and opaques (Fe-Ti oxides) are the retrograde minerals. The olivine inclusion in a plagioclase (Fig. 6e) and plagioclase inclusion in a clinopyroxene (Fig. 6f) indicate that the crystallization order for the cumulate gabbros of the Kuluncak (Malatya) ophiolite is olivine, plagioclase, clinopyroxene, orthopyroxene and amphibole. Petrographic features of the cumulate rocks are given in Table 1, and the results of microprobe analyses are summarized below (Tables 3, 4, 5, 6, 7).

Table 1 - Summary of petrographic features of the mafic cumulate rocks of the Kuluncak (Malatya) ophiolite.

Sample	Easting	Northing	Rock Type	Texture	*Mode (%)*						Crystal shape*					
					Ol	Cpx	Opx	Pl	Amp	Opq	Ol	Cpx	Opx	Pl	Amp	Opq
H1	408853	4295561	Olivine Gabbro	Mesocumulate	15	33		50		2	4	4		4		4
H3	409470	4292319	Olivine Gabbro	Mesocumulate	12	38		47		3	4	2		4		4
H4	409277	4292171	Gabbro	Mesocumulate	8	38		51	1	2	4	4		4	4	4
H6	408888	4290872	Gabbro	Mesocumulate	7	36		57			4	4		4		
H7	408699	4290933	Olivine Gabbro	Mesocumulate	14	34		48	1	3	2	2		4	4	4
H9	409315	4293297	Olivine Gabbro	Mesocumulate	15	29		55		1	2	2		4		4
H11	409271	4293509	Gabbro	Mesocumulate		39		60		1		2		2		4
H12	408960	4293293	Olivine Gabbro	Mesocumulate	19	29		48	2	2	2	2		4	4	4
H13	409093	4293656	Olivine Gabbro	Mesocumulate	15	30	2	52		1	4	4	4	2		4
H14	408417	4296126	Olivine Gabbro	Mesocumulate	15	43		40	1	1	2	2		4	4	4
H15	408407	4296339	Olivine Gabbro	Mesocumulate	25	21	2	48	2	2	2	2	4	2	4	4
H19	405815	4295550	Olivine Gabbro	Mesocumulate	10	40		47	1	2	2	2		2	4	4
H20	405429	4295262	Olivine Gabbro	Mesocumulate	18	29		49	2	2	2	4		4	4	4
H23	407404	4295545	Gabbro	Orthocumulate		39		60		1		2		2		4
H27	404561	4296339	Gabbro	Mesocumulate	5	40		49	2	4	2	2		2	4	4
H28	404528	4296140	Gabbro	Mesocumulate		32		64		4		4		2		4
H30	405220	4296530	Olivine Gabbro	Orthocumulate	10	38		49		3	4	2		2		4
H32	404605	4306604	Gabbro	Mesocumulate	5	51		43		1	4	4		2		4
H33	404385	4306579	Olivine Gabbro	Mesocumulate	20	36		40	2	2	2	2		2	4	4
H34	404540	4306670	Olivine Gabbro	Mesocumulate	24	34		40		2	4	4		4		4
H35	403428	4306920	Gabbro	Orthocumulate		36		62	2			4		4	4	
H40	408415	4295557	Olivine Gabbro	Mesocumulate	15	33		50		2	2	2		2		4
H41	408249	4295893	Olivine Gabbro	Mesocumulate	15	30		53		2	4	2		2		4
H45	401505	4297537	Gabbro	Mesocumulate		41		51	3	5		4		4	4	4
H46	401617	4297563	Gabbro	Orthocumulate		51		43	3	3		4		2	4	4

*1: euhedral to subhedral; 2: subhedral to anhedral; 3: subhedral; 4: anhedral; 5: euhedral; 6: euhedral to anhedral.

Ol: olivine; Cpx: clinopyroxene; Opx: orthopyroxene; Pl: plagioclase; Amp: amphibole; Opq: opaque

Olivine

The olivines are unzoned and have Fo contents of 65.2 in gabbros and from 72.5 to 86.9 in olivine gabbros. The NiO content decreases from olivine gabbros to gabbros and varies within the range 0.10-0.16 wt% in the mafic cumulates (Table 3).

Clinopyroxene

The clinopyroxenes are unzoned, and their compositions are shown in the pyroxene quadrilateral in Fig. 7a. In terms of the quadrilateral components, cumulus clinopyroxene composition is $En_{43.2-55.4}Fs_{4.2-14.3}Wo_{35.8-48.1}$ in olivine gabbro and $En_{41.6-47.4}Fs_{6.8-14.3}Wo_{41.7-47.4}$ in gabbros. The clinopyroxenes crystallizing in cumulates have diopsidic to augitic

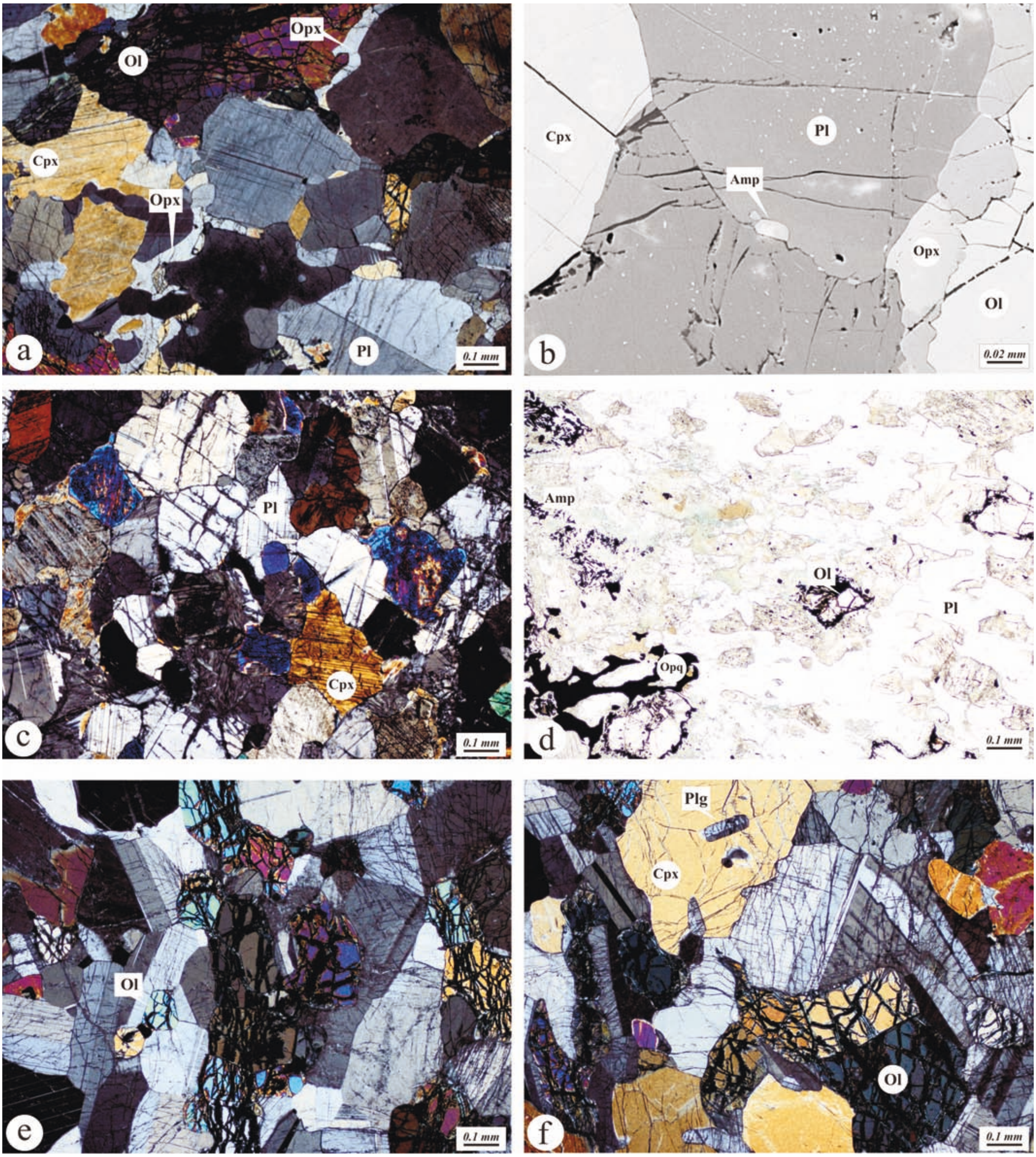

Fig. 6 - Microstructure of the mafic cumulate rocks of the Kuluncak (Malatya) ophiolite: (a, b) mesocumulate olivine gabbro; (c) mesocumulate gabbro; (d) amphibole replacing the clinopyroxene in gabbro; (e) subhedral olivine included in plagioclase; (f) euhedral plagioclase included in clinopyroxene. Cross-polarized light (a, c, e, f), plane-polarized light (d) and back-scattered electron image (b). Mineral abbreviation from Whitney and Evans (2010).

Table 2 - Major (wt%) and trace (ppm) element contents of mafic cumulate rocks of the Kuluncak (Malatya) ophiolite.

	Olivine Gabbro															Gabbro									
Sample	**H1**	**H3**	**H7**	**H9**	**H12**	**H13**	**H14**	**H15**	**H19**	**H20**	**H30**	**H33**	**H34**	**H40**	**H41**	**H4**	**H6**	**H11**	**H23**	**H27**	**H28**	**H32**	**H35**	**H45**	**H46**
SiO_2	46.43	46.59	46.98	46.54	47.99	45.65	47.38	45.37	47.05	48.07	46.87	45.73	45.82	42.46	44.16	46.96	45.78	47.01	46.93	48.28	47.75	45.08	46.92	50.58	48.58
TiO_2	0.08	0.08	0.07	0.07	0.17	0.08	0.24	0.12	0.17	0.16	0.40	0.12	0.16	0.03	0.06	0.19	0.13	0.22	0.08	0.36	0.36	0.11	0.19	0.59	0.56
Al_2O_3	16.36	16.42	17.49	17.08	16.12	20.36	14.43	17.29	17.22	16.49	15.26	17.98	12.86	20.43	15.81	16.94	17.01	15.70	20.83	16.23	18.91	27.76	18.37	15.25	16.16
Cr_2O_3	0.09	0.11	0.09	0.07	0.12	0.05	0.11	0.08	0.08	0.08	0.09	0.11	0.15	0.16	0.12	0.04	0.08	0.07	0.07	0.04	0.02	0.02	0.05	<0.01	0.07
tFe_2O_3	4.16	4.06	5.60	3.94	6.59	3.29	5.63	7.71	6.40	6.67	9.91	5.52	7.64	3.58	6.07	6.03	4.91	5.06	3.41	7.76	6.48	3.30	5.65	8.44	8.21
MnO	0.08	0.08	0.10	0.07	0.12	0.06	0.11	0.12	0.12	0.12	0.16	0.09	0.13	0.06	0.10	0.11	0.10	0.09	0.06	0.14	0.12	0.05	0.10	0.10	0.14
MgO	12.99	10.85	11.80	13.21	11.63	9.02	11.84	13.01	10.83	10.52	11.23	12.47	16.23	12.77	15.16	9.29	10.6	11.08	7.66	9.12	6.71	4.40	8.79	8.76	8.71
CaO	16.42	17.38	15.47	15.50	14.73	16.61	16.74	12.74	15.74	15.59	13.31	14.23	13.31	13.96	14.00	15.45	15.00	16.73	16.50	14.99	14.56	13.23	14.75	9.19	13.09
Na_2O	0.56	0.88	0.91	0.67	1.39	1.23	0.96	1.15	1.06	1.15	1.38	0.89	0.69	0.83	0.45	1.58	1.81	0.77	1.70	1.64	2.39	1.39	1.43	3.14	2.09
K_2O	0.02	<0.01	<0.01	<0.01	0.01	<0.01	<0.01	<0.01	<0.01	<0.01	0.02	0.11	0.02	0.04	<0.01	<0.01	0.02	0.10	0.05	0.04	0.02	1.48	0.70	0.39	0.10
P_2O_5	<0.01	<0.01	<0.01	<0.01	0.02	<0.01	0.02	<0.01	<0.01	<0.01	0.01	<0.01	0.01	0.01	<0.01	<0.01	<0.01	<0.01	<0.01	<0.01	0.01	<0.01	0.01	0.05	0.04
LOI	2.50	3.30	1.20	2.60	0.90	3.40	2.30	2.10	1.10	0.90	1.10	2.50	2.60	5.40	3.80	3.20	4.30	2.90	2.50	1.20	2.50	3.10	2.80	3.30	2.10
Total	99.77	99.77	99.77	99.76	99.79	99.82	99.75	99.75	99.78	99.78	99.77	99.76	99.69	99.77	99.73	99.81	99.78	99.78	99.84	99.80	99.84	99.90	99.81	99.80	99.80
Mg#	86.1	84.1	80.7	86.9	77.8	84.5	80.6	77.0	77.0	75.8	69.2	81.7	80.8	87.6	83.2	75.3	81.1	81.3	81.7	70.0	67.2	72.5	75.5	67.3	67.8
Ba	5	2	2	2	3	7	2	2	3	2	6	3	6	6	<1	2	4	4	9	8	4	24	12	59	12
Rb	0.3	0.2	0.2	0.4	0.1	<0.1	0.3	0.2	0.2	0.2	0.3	6.6	1.5	1.1	0.1	0.2	0.5	1.9	1.4	0.3	0.2	76.6	22.4	5.8	0.8
Sr	125.7	160.7	87.6	86	105.3	292.9	252.3	108	107.9	122.5	111.5	82.7	51.1	159.1	80	130	322	209.7	192.2	125.2	212.3	187.4	163.7	143.9	137
Y	2.5	2.7	2.1	2.2	5.1	2.3	6.1	2.8	4.7	5.1	8.8	3.2	4.8	0.7	1.6	5.4	3.9	6	2.2	9.6	8.5	2.6	5.8	13.2	15.4
Zr	1.3	1	0.8	1.1	2.4	1.1	2.4	1.6	2.2	2	9.5	2.8	2.6	2.1	1	1.9	2.8	3.1	1.6	6.2	7.7	2.2	2.4	22.7	30.4
Nb	<0.1	<0.1	<0.1	<0.1	<0.1	<0.1	<0.1	<0.1	<0.1	<0.1	<0.1	<0.1	<0.1	<0.1	<0.1	<0.1	0.6	<0.1	<0.1	<0.1	<0.1	<0.1	<0.1	0.2	<0.1
Th	<0.2	<0.2	<0.2	<0.2	<0.2	<0.2	<0.2	<0.2	<0.2	<0.2	<0.2	<0.2	<0.2	<0.2	<0.2	<0.2	<0.2	<0.2	<0.2	<0.2	<0.2	<0.2	<0.2	<0.2	<0.2
Pb	0.2	0.2	0.1	0.2	0.2	<0.1	0.2	0.2	0.2	0.3	0.3	<0.1	0.1	<0.1	0.1	0.1	0.3	<0.1	0.3	<0.1	0.2	4.8	0.3	<0.1	0.2
Ga	8.4	8	10.4	8.9	11.3	10.8	9.5	10.8	11.4	10.9	11.5	9.7	8	8.7	7.8	11.4	10.1	10.6	11.6	13	15.3	14.7	13.2	12.5	13.4
Zn	9	9	12	8	13	5	9	28	12	11	19	20	27	10	18	13	10	3	4	16	8	25	10	3	10
Cu	9.2	172.7	141.8	131.1	3.6	8.2	113.9	78.2	131.3	146.9	93.8	138.7	142.4	55	117.5	134.1	11.2	2.9	159.2	103.6	26.7	39.8	76	1.4	118
Ni	131.7	135.7	176.8	156.5	124.8	59	98.7	241.3	116.2	98.7	124.3	230.2	298.7	427.6	284.3	69	66.9	37.9	44.6	57.7	21.2	82.4	59.3	14.6	48.2
V	112	124	105	86	140	97	199	85	166	158	198	91	135	35	83	167	138	174	95	213	203	52	153	336	210
Cr	643.1	752.6	595.3	499.5	807.4	321.6	766.3	561.0	513.2	561.0	615.8	745.8	1033.1	1067.4	821.0	301.0	513.2	465.3	506.3	253.2	150.5	136.8	355.8	13.7	465.3
Hf	<0.1	<0.1	<0.1	<0.1	<0.1	<0.1	<0.1	<0.1	<0.1	<0.1	0.3	<0.1	<0.1	<0.1	<0.1	0.1	0.2	0.1	<0.1	0.3	0.3	0.2	0.1	0.8	1
Cs	<0.1	<0.1	<0.1	<0.1	<0.1	<0.1	<0.1	<0.1	<0.1	<0.1	<0.1	1.7	0.8	<0.1	<0.1	<0.1	<0.1	<0.1	0.1	<0.1	<0.1	5.3	0.5	<0.1	<0.1
Sc	38	43	33	33	41	32	59	25	44	41	39	30	41	15	29	45	40	52	32	47	40	10	37	40	40
Ta	<0.1	<0.1	0.2	<0.1	<0.1	<0.1	<0.1	<0.1	<0.1	<0.1	<0.1	<0.1	<0.1	<0.1	<0.1	<0.1	0.4	<0.1	<0.1	<0.1	<0.1	<0.1	<0.1	<0.1	<0.1
Co	41	36.5	50.2	45.2	46	29.3	39.1	63.6	47.1	48.3	61.5	46.8	69.1	44.4	59.6	42.6	39.3	36.9	25.4	42.4	29.7	21.5	36.5	41.3	40.7
U	<0.1	<0.1	<0.1	<0.1	<0.1	<0.1	<0.1	<0.1	<0.1	<0.1	<0.1	<0.1	<0.1	<0.1	<0.1	<0.1	<0.1	<0.1	<0.1	<0.1	<0.1	<0.1	<0.1	<0.1	<0.1
W	1.2	<0.5	<0.5	<0.5	<0.5	<0.5	<0.5	<0.5	<0.5	<0.5	<0.5	<0.5	<0.5	<0.5	<0.5	<0.5	<0.5	<0.5	<0.5	0.6	<0.5	<0.5	<0.5	<0.5	1.1
Sn	<1	<1	<1	<1	<1	<1	<1	<1	<1	<1	<1	<1	<1	<1	<1	<1	<1	<1	<1	<1	<1	<1	<1	<1	<1
Mo	0.2	<0.1	0.1	<0.1	0.1	<0.1	0.1	0.1	0.1	0.1	0.2	<0.1	<0.1	<0.1	<0.1	<0.1	<0.1	<0.1	<0.1	0.1	0.1	<0.1	<0.1	<0.1	<0.1
Au	<0.5	7.1	<0.5	1.7	<0.5	11.6	1	0.6	<0.5	<0.5	<0.5	5.2	1	<0.5	14.7	<0.5	<0.5	<0.5	<0.5	<0.5	1.3	<0.5	<0.5	<0.5	<0.5
La	0.10	0.10	0.10	0.10	0.10	<0.1	0.20	0.10	0.30	0.10	0.90	0.60	0.40	0.40	0.30	0.20	0.20	0.10	0.30	0.40	0.40	0.50	0.20	1.10	1.10
Ce	0.30	0.30	0.20	0.20	0.40	<0.1	0.40	0.30	0.30	0.40	1.50	0.40	0.50	0.10	0.10	0.40	0.60	0.40	0.30	1.10	1.10	0.60	0.40	3.50	3.60
Pr	0.05	0.04	0.04	0.05	0.09	0.04	0.11	0.07	0.09	0.08	0.27	0.07	0.09	0.02	0.02	0.10	0.09	0.10	0.07	0.23	0.22	0.10	0.09	0.61	0.67
Nd	<0.3	<0.3	<0.3	<0.3	0.40	<0.3	1.10	0.50	0.60	0.60	1.30	0.60	0.40	<0.3	<0.3	0.50	0.40	0.90	<0.3	1.40	1.50	0.50	0.70	3.00	4.10
Sm	0.19	0.15	0.13	0.17	0.37	0.16	0.48	0.27	0.33	0.33	0.78	0.23	0.34	0.07	0.12	0.40	0.29	0.47	0.19	0.80	0.68	0.20	0.39	1.21	1.52
Eu	0.12	0.11	0.16	0.13	0.26	0.15	0.26	0.23	0.22	0.24	0.43	0.18	0.20	0.07	0.09	0.27	0.17	0.25	0.14	0.45	0.42	0.22	0.29	0.50	0.57
Gd	0.31	0.29	0.25	0.29	0.64	0.31	0.88	0.43	0.60	0.63	1.24	0.45	0.69	0.11	0.19	0.79	0.49	0.8	0.32	1.31	1.07	0.31	0.67	1.70	2.18
Tb	0.07	0.06	0.06	0.06	0.16	0.07	0.18	0.09	0.13	0.13	0.24	0.10	0.14	0.02	0.04	0.15	0.11	0.17	0.06	0.26	0.24	0.07	0.15	0.35	0.44
Dy	0.39	0.47	0.44	0.41	1.10	0.44	1.10	0.56	0.84	0.92	1.65	0.62	0.81	0.13	0.29	1.02	0.68	1.18	0.37	1.78	1.53	0.45	1.18	2.28	2.71
Ho	0.10	0.10	0.11	0.08	0.21	0.11	0.25	0.13	0.20	0.19	0.35	0.13	0.19	0.04	0.07	0.21	0.15	0.29	0.09	0.37	0.34	0.11	0.21	0.52	0.61
Er	0.25	0.27	0.23	0.22	0.59	0.26	0.76	0.35	0.59	0.68	1.04	0.39	0.63	0.06	0.22	0.56	0.44	0.82	0.31	1.16	0.99	0.28	0.64	1.63	1.79
Tm	0.04	0.05	0.04	0.03	0.08	0.04	0.10	0.05	0.09	0.09	0.15	0.05	0.08	0.01	0.03	0.10	0.06	0.11	0.05	0.17	0.14	0.05	0.11	0.25	0.29
Yb	0.15	0.20	0.19	0.20	0.52	0.22	0.59	0.33	0.48	0.41	0.85	0.24	0.52	0.08	0.15	0.46	0.40	0.58	0.14	0.98	0.76	0.29	0.55	1.47	1.76
Lu	0.04	0.04	0.03	0.03	0.09	0.04	0.11	0.05	0.07	0.08	0.15	0.04	0.08	0.02	0.02	0.09	0.06	0.09	0.03	0.15	0.15	0.04	0.10	0.22	0.26
Ce_N/Sm_N	0.39	0.50	0.38	0.29	0.27	-	0.21	0.28	0.23	0.30	0.48	0.43	0.37	0.36	0.21	0.25	0.52	0.21	0.39	0.34	0.40	0.75	0.26	0.72	0.59
Ce_N/Yb_N	0.56	0.42	0.29	0.28	0.21	-	0.19	0.25	0.17	0.27	0.49	0.46	0.27	0.35	0.19	0.24	0.42	0.19	0.60	0.31	0.40	0.57	0.20	0.66	0.57

tFe_2O_3 represents total iron oxide as ferric iron; LOI, loss on ignition; Mg#, (Mg x 100)/(Mg+Fe_{tot}).

Table 3 - Representative analyses of major elements for olivines in the mafic cumulate rocks.

	Olivine Gabbro												Gabbro		
	H9-C1/4	**H9-D1/2**	**H9-E1/5**	**H13-B1/1**	**H13-D1/2**	**H13-D1/4**	**H15-A1/1**	**H15-A1/3**	**H15-B1/2**	**H19-D1/1**	**H19-C1/3**	**H19-E1/4**	**H27-E1/2**	**H27-C1/1**	**H27-E1/5**
SiO_2	40.45	40.78	40.42	40.13	39.83	39.29	37.83	37.88	38.58	38.26	38.00	37.52	36.66	36.09	36.50
TiO_2	bdl	bdl	bdl	bdl	bdl	bdl	bdl	bdl	bdl	bdl	bdl	bdl	bdl	bdl	bdl
Al_2O_3	bdl	bdl	bdl	bdl	bdl	0.81	bdl	bdl	bdl	bdl	bdl	bdl	bdl	bdl	bdl
FeO*	12.56	13.02	13.34	15.43	16.36	17.10	21.16	21.13	21.59	23.74	24.47	25.17	29.37	30.05	31.76
Cr_2O_3	bdl	bdl	bdl	bdl	bdl	bdl	bdl	bdl	bdl	bdl	bdl	bdl	bdl	bdl	bdl
MnO	0.19	0.20	0.27	0.25	0.27	0.20	0.25	0.38	0.36	0.32	0.33	0.29	0.38	0.48	0.48
MgO	46.83	46.25	46.39	43.81	43.50	41.82	40.77	40.00	39.30	37.35	36.96	37.31	32.42	32.18	31.28
CaO	bdl	bdl	bdl	bdl	bdl	0.21	bdl	bdl	bdl	bdl	bdl	bdl	0.07	bdl	bdl
Na_2O	bdl	bdl	bdl	bdl	bdl	bdl	bdl	bdl	bdl	bdl	bdl	bdl	bdl	bdl	bdl
K_2O	0.02	0.02	0.03	0.02	bdl	0.02	bdl	bdl	bdl	bdl	bdl	bdl	bdl	bdl	bdl
NiO	0.12	bdl	0.16	0.11	0.13	bdl	0.13	bdl	0.13	bdl	bdl	bdl	bdl	0.10	bdl
Total	100.23	100.40	100.64	99.81	100.21	99.56	100.20	99.54	100.02	99.81	99.92	100.42	99.09	99.00	100.12
Si	1.002	1.009	1.001	1.011	1.004	1.000	0.979	0.987	1.000	1.004	1.000	0.987	0.999	0.990	0.995
Ti	0.000	0.000	0.000	0.000	0.000	0.000	0.000	0.000	0.000	0.000	0.000	0.000	0.000	0.000	0.000
Al	0.000	0.000	0.000	0.000	0.000	0.024	0.000	0.000	0.000	0.000	0.000	0.000	0.000	0.000	0.000
Fe	0.260	0.269	0.276	0.325	0.345	0.364	0.458	0.460	0.468	0.521	0.538	0.554	0.669	0.689	0.724
Cr	0.000	0.000	0.000	0.000	0.000	0.000	0.000	0.000	0.000	0.000	0.000	0.000	0.000	0.000	0.000
Mn	0.004	0.004	0.006	0.005	0.006	0.004	0.005	0.008	0.008	0.007	0.007	0.006	0.009	0.011	0.011
Mg	1.729	1.706	1.712	1.645	1.635	1.587	1.573	1.553	1.519	1.461	1.450	1.463	1.317	1.315	1.271
Ca	0.000	0.000	0.000	0.000	0.000	0.006	0.000	0.000	0.000	0.000	0.000	0.000	0.002	0.000	0.000
Na	0.000	0.000	0.000	0.000	0.000	0.000	0.000	0.000	0.000	0.000	0.000	0.000	0.000	0.000	0.000
K	0.001	0.001	0.001	0.001	0.000	0.001	0.000	0.000	0.000	0.000	0.000	0.000	0.000	0.000	0.000
Ni	0.005	0.000	0.006	0.004	0.005	0.000	0.005	0.000	0.005	0.000	0.000	0.000	0.000	0.004	0.000
Total	3.001	2.993	3.003	2.992	2.998	2.990	3.023	3.014	3.002	2.998	3.002	3.015	3.002	3.013	3.006
Fo (mol%)	86.9	86.4	86.1	83.5	82.6	81.3	77.5	77.1	76.4	73.7	72.9	72.5	66.3	65.6	63.7

Number of ions on the basis of 4 (O); *total Fe is expressed as FeO; bdl, below detection limit.

Table 4 - Representative analyses of major elements for clinopyroxenes in the mafic cumulate rocks.

	Olivine Gabbro								Gabbro					
	H9-D1/6r	H9-D1/4	H13-B1/8r	H13-A1/5	H15-A1/5	H15-D1/4	H19-E1/1	H19-D1/2	H6-C1/7r	H6-B1/3	H6-C1/5	H27-E1/3	H27-C1/5	H27-B1/3
SiO_2	54.50	53.55	52.85	53.42	52.80	51.46	51.87	52.44	53.37	53.08	52.39	52.72	52.28	50.99
Al_2O_3	0.63	2.52	1.95	2.27	2.33	3.13	2.57	2.28	2.33	2.15	2.59	1.54	1.98	2.45
TiO_2	bdl	0.20	0.28	0.25	0.44	0.48	0.42	0.34	0.14	0.30	0.32	0.40	0.38	0.73
FeO*	2.75	5.45	4.06	5.79	5.11	6.50	5.50	8.65	4.12	5.44	6.59	7.49	8.13	8.57
MnO	bdl	0.15	0.17	0.16	0.14	0.13	bdl	0.18	0.13	bdl	0.18	0.18	0.20	0.24
MgO	17.99	19.95	16.50	17.89	15.34	16.16	15.09	17.26	16.09	15.84	16.54	15.24	14.85	14.39
Cr_2O_3	0.12	0.25	0.21	0.15	0.43	0.51	0.20	0.20	0.11	0.24	0.23	bdl	bdl	0.11
CaO	24.11	17.95	23.31	20.80	23.59	21.17	23.20	17.40	23.14	22.77	20.21	22.43	21.79	21.20
Na_2O	0.13	0.21	0.32	0.26	0.37	0.39	0.27	0.21	0.25	0.29	0.31	0.29	0.29	0.32
K_2O	bdl	bdl	bdl	bdl	bdl	0.02	bdl	bdl	0.02	bdl	bdl	bdl	bdl	bdl
NiO	bdl	bdl	bdl	bdl	bdl	bdl	bdl	bdl	bdl	bdl	bdl	bdl	bdl	bdl
Total	100.30	100.26	99.67	101.05	100.56	99.94	99.23	98.97	99.74	100.23	99.37	100.39	100.02	99.03
Si	1.971	1.931	1.935	1.927	1.929	1.888	1.922	1.947	1.955	1.943	1.932	1.941	1.936	1.912
Al^{IV}	0.029	0.069	0.065	0.073	0.071	0.112	0.078	0.053	0.045	0.057	0.068	0.059	0.064	0.088
Al^{VI}	0.001	0.038	0.019	0.023	0.029	0.024	0.034	0.047	0.056	0.036	0.045	0.008	0.023	0.020
Ti	0.000	0.005	0.008	0.007	0.012	0.013	0.012	0.009	0.004	0.008	0.009	0.011	0.011	0.021
Fe^{3+}	0.036	0.029	0.049	0.052	0.032	0.076	0.035	0.001	0.001	0.018	0.021	0.049	0.040	0.049
Fe^{2+}	0.047	0.135	0.075	0.123	0.125	0.124	0.136	0.271	0.128	0.148	0.182	0.182	0.211	0.220
Mn	0.000	0.005	0.005	0.005	0.004	0.004	0.000	0.006	0.004	0.000	0.006	0.006	0.006	0.008
Mg	0.970	1.072	0.900	0.962	0.836	0.884	0.834	0.956	0.879	0.864	0.909	0.836	0.820	0.804
Cr	0.003	0.007	0.006	0.004	0.012	0.015	0.006	0.006	0.003	0.007	0.007	0.000	0.000	0.003
Ca	0.934	0.693	0.914	0.804	0.923	0.832	0.921	0.692	0.908	0.893	0.799	0.885	0.865	0.851
Na	0.009	0.014	0.022	0.018	0.026	0.028	0.019	0.015	0.018	0.021	0.022	0.021	0.021	0.023
K	0.000	0.000	0.000	0.000	0.000	0.001	0.000	0.000	0.001	0.000	0.000	0.000	0.000	0.000
Ni	0.000	0.000	0.000	0.000	0.000	0.000	0.000	0.000	0.000	0.000	0.000	0.000	0.000	0.000
Total	4.000	4.000	4.000	4.000	4.000	4.000	4.000	4.000	4.000	4.000	4.000	4.000	4.000	4.000
Ens.	48.8	55.4	46.3	49.5	43.5	46.0	43.2	49.7	45.8	44.8	47.4	42.7	42.2	41.6
Fs.	4.2	8.7	6.7	9.2	8.4	10.6	9.0	14.3	6.8	8.8	10.9	12.1	13.3	14.3
Wol.	47.0	35.8	47.0	41.3	48.1	43.4	47.8	36.0	47.4	46.3	41.7	45.2	44.5	44.1
Total	100.0	100.0	100.0	100.0	100.0	100.0	100.0	100.0	100.0	100.0	100.0	100.0	100.0	100.0
Mg#	92.1	86.7	87.9	84.6	84.3	81.6	83.0	77.8	87.2	83.9	81.7	78.4	76.5	75.0

Number of ions on the basis of 6 (O); *total Fe is expressed as FeO; bdl, below detection limit; r = rim.

Table 5 - Representative analyses of major elements for orthopyroxenes in the mafic cumulate rocks.

	Olivine Gabbro														
	H13-B1/1	H13-B1/2	H13-B1/3	H13-B1/4r	H13-B1/5r	H15-B1/1	H15-B1/2	H15-B1/3	H15-B1/4	H15-B1/5	H15-D1/1	H15-D1/2	H15-D1/3	H15-D1/4	H15-D1/5
SiO_2	56.34	56.32	56.50	56.28	56.15	54.91	54.93	54.96	55.24	54.84	54.91	54.64	54.04	54.57	54.92
Al_2O_3	1.11	1.16	1.19	1.18	1.29	1.14	1.33	0.98	1.07	1.30	1.49	1.55	1.58	1.68	1.78
TiO_2	0.07	0.12	0.07	0.11	0.13	bdl	0.10	bdl	0.05	0.08	0.21	0.24	0.21	0.20	0.11
FeO*	10.50	10.16	10.23	10.41	10.51	13.70	13.34	13.68	13.68	13.47	13.15	13.04	13.32	13.97	13.18
MnO	0.22	0.22	0.20	0.22	0.30	0.33	0.29	0.38	0.27	0.37	0.26	0.33	0.31	0.30	0.28
MgO	31.24	30.86	31.08	31.42	30.62	29.41	29.14	29.45	29.12	29.54	28.39	28.37	28.46	28.64	28.47
Cr_2O_3	0.14	0.12	0.09	0.13	0.11	bdl	bdl	bdl	bdl	bdl	0.18	0.16	0.21	0.23	0.16
CaO	0.71	0.65	0.40	0.64	0.89	0.38	0.52	0.38	0.47	0.49	0.94	0.78	0.94	0.89	0.42
Na_2O	bdl	bdl	bdl	bdl	bdl	bdl	0.07	bdl	bdl	bdl	bdl	bdl	bdl	bdl	bdl
K_2O	bdl	bdl	bdl	bdl	bdl	bdl	0.02	bdl	bdl	bdl	bdl	bdl	bdl	bdl	bdl
NiO	bdl	bdl	bdl	bdl	bdl	bdl	bdl	bdl	bdl	bdl	bdl	bdl	bdl	bdl	bdl
Total	100.42	99.63	99.80	100.46	100.03	99.95	99.82	99.90	100.02	100.12	99.61	99.15	99.09	100.56	99.38
Si	1.973	1.989	1.990	1.969	1.978	1.956	1.958	1.958	1.968	1.948	1.968	1.967	1.946	1.939	1.970
Al^{IV}	0.027	0.011	0.010	0.031	0.022	0.044	0.042	0.042	0.032	0.052	0.032	0.033	0.054	0.061	0.030
Al^{VI}	0.019	0.037	0.040	0.018	0.032	0.003	0.014	0.000	0.013	0.002	0.031	0.033	0.013	0.010	0.046
Ti	0.002	0.003	0.002	0.003	0.003	0.000	0.003	0.000	0.001	0.002	0.006	0.006	0.006	0.005	0.003
Fe^{3+}	0.003	0.035	0.036	0.006	0.018	0.041	0.028	0.042	0.019	0.044	0.013	0.017	0.026	0.037	0.023
Fe^{2+}	0.304	0.335	0.337	0.299	0.327	0.367	0.369	0.366	0.388	0.356	0.407	0.409	0.375	0.378	0.418
Mn	0.007	0.007	0.006	0.007	0.009	0.010	0.009	0.011	0.008	0.011	0.008	0.010	0.009	0.009	0.009
Mg	1.631	1.625	1.632	1.639	1.608	1.561	1.549	1.565	1.547	1.564	1.517	1.523	1.528	1.517	1.523
Cr	0.004	0.003	0.003	0.004	0.003	0.000	0.000	0.000	0.000	0.000	0.005	0.005	0.006	0.006	0.005
Ca	0.027	0.025	0.015	0.024	0.034	0.014	0.020	0.015	0.018	0.019	0.036	0.030	0.036	0.034	0.016
Na	0.000	0.000	0.000	0.000	0.000	0.000	0.005	0.000	0.000	0.000	0.000	0.000	0.000	0.000	0.000
K	0.000	0.000	0.000	0.000	0.000	0.000	0.001	0.000	0.000	0.000	0.000	0.000	0.000	0.000	0.000
Ni	0.000	0.000	0.000	0.000	0.000	0.000	0.000	0.000	0.000	0.000	0.000	0.000	0.000	0.000	0.000
Total	4.000	4.000	4.000	4.000	4.000	4.000	4.000	4.000	4.000	4.000	4.000	4.000	4.000	4.000	4.000
Ens.	82.7	83.1	83.5	83.0	82.0	78.3	78.4	78.3	78.1	78.4	77.6	77.9	77.4	76.8	78.4
Fs.	15.9	15.7	15.7	15.8	16.3	21.0	20.6	21.0	21.0	20.6	20.6	20.6	20.8	21.5	20.8
Wol.	1.4	1.3	0.8	1.2	1.7	0.7	1.0	0.7	0.9	0.9	1.8	1.5	1.8	1.7	0.8
Total	100.0	100.0	100.0	100.0	100.0	100.0	100.0	100.0	100.0	100.0	100.0	100.0	100.0	100.0	100.0
Mg #	84.1	81.4	81.4	84.3	82.3	79.3	79.6	79.3	79.1	79.6	78.3	78.2	79.2	78.5	77.6

Number of ions on the basis of 6 (O); *total Fe is expressed as FeO; bdl, below detection limit; r = rim.

Table 6 - Representative analyses of major elements for plagioclases in the mafic cumulate rocks.

	Olivine Gabbro								Gabbro			
	H9-C1/6r	**H9-C1/1**	**H13-D1/6r**	**H13-C1/2**	**H15-B1/22**	**H15-D1/5**	**H19-E1/6r**	**H19-D1/2**	**H6-B1/8r**	**H6-C1/4**	**H27-E1/5**	**H27-E1/4**
SiO_2	45.55	46.24	45.74	47.26	44.15	48.68	45.27	48.19	46.50	48.44	48.42	49.25
Al_2O_3	34.77	34.33	35.17	33.53	35.43	32.49	33.43	32.84	34.20	33.40	32.31	31.68
TiO_2	bdl	bdl	bdl	bdl	bdl	bdl	bdl	bdl	bdl	bdl	bdl	bdl
FeO*	0.26	0.18	0.27	0.21	0.25	0.21	0.89	0.22	0.20	0.27	0.34	0.40
MnO	bdl	bdl	bdl	bdl	bdl	bdl	bdl	bdl	bdl	bdl	bdl	bdl
MgO	bdl	bdl	bdl	bdl	bdl	bdl	1.61	bdl	bdl	bdl	bdl	bdl
CaO	18.33	17.69	18.21	17.13	19.46	16.17	17.42	16.56	17.84	16.60	16.04	15.31
Na_2O	1.09	1.55	1.23	1.92	0.72	2.76	1.33	2.51	1.49	2.22	2.54	3.06
K_2O	0.02	bdl	bdl	bdl	bdl	bdl	0.02	bdl	bdl	0.02	bdl	bdl
Total	100.10	100.02	100.64	100.06	99.91	100.38	100.02	100.34	100.25	101.04	99.73	99.78
Si	2.098	2.125	2.092	2.167	2.036	2.216	2.075	2.197	2.133	2.198	2.222	2.253
Al	1.887	1.859	1.896	1.812	1.926	1.743	1.806	1.764	1.849	1.786	1.748	1.708
Ti	0.000	0.000	0.000	0.000	0.000	0.000	0.000	0.000	0.000	0.000	0.000	0.000
Fe^{2+}	0.010	0.007	0.010	0.008	0.010	0.008	0.034	0.008	0.008	0.010	0.013	0.015
Mn	0.000	0.000	0.000	0.000	0.000	0.000	0.000	0.000	0.000	0.000	0.000	0.000
Mg	0.000	0.000	0.000	0.000	0.000	0.000	0.110	0.000	0.000	0.000	0.000	0.000
Ca	0.904	0.871	0.892	0.842	0.962	0.789	0.855	0.809	0.877	0.807	0.789	0.750
Na	0.097	0.138	0.109	0.171	0.064	0.244	0.118	0.222	0.133	0.195	0.226	0.271
K	0.001	0.000	0.000	0.000	0.000	0.000	0.001	0.000	0.000	0.001	0.000	0.000
Total	5.000	5.000	5.000	5.000	5.000	5.000	5.000	5.000	5.000	5.000	5.000	5.000
Or	0.1	0.1	0.0	0.1	0.1	0.1	0.1	0.1	0.1	0.1	0.0	0.1
Ab	9.7	13.7	10.9	16.9	6.3	23.6	12.1	21.5	13.1	19.5	22.3	26.5
An	90.2	86.3	89.1	83.1	93.7	76.4	87.8	78.4	86.8	80.4	77.7	73.4

Number of ions on the basis of 16 (O); *total Fe is expressed as FeO; bdl, below detection limit; r represent rim.

Table 7 - Representative analyses of major elements for amphiboles in the mafic cumulate rocks.

	Olivine Gabbro			Gabbro										
	Pargasitic Hornblende			Tschermakitic Hornblende						Tschermakite				
	H15-B1/1	**H15-B1/2**	**H15-B1/3**	**H27-B1/4**	**H27-C1/1**	**H27-C1/2**	**H27-C1/3**	**H27-C1/4**	**H27-C1/5**	**H27-E1/1**	**H27-E1/2**	**H27-E1/3**	**H27-E1/4**	**H27-E1/5**
SiO_2	44.45	43.65	44.27	44.47	44.52	44.19	44.02	44.58	44.24	43.83	44.29	43.16	43.07	42.96
Al_2O_3	15.10	13.31	12.02	13.06	10.70	10.62	10.61	10.86	10.63	13.60	13.60	14.49	14.77	14.95
TiO_2	0.52	0.60	0.60	0.08	2.20	2.54	2.55	2.27	2.51	0.07	0.04	0.05	0.05	0.04
FeO*	8.20	8.79	8.44	11.05	11.64	11.29	11.38	10.60	11.47	10.92	11.57	11.32	11.11	11.19
MnO	bdl	bdl	bdl	0.16	bdl	0.21	0.13	bdl	bdl	0.25	0.19	0.25	0.23	0.18
MgO	14.55	15.42	16.10	15.02	14.71	14.54	14.60	14.98	14.67	15.05	14.72	14.08	14.35	13.82
Cr_2O_3	bdl	bdl	bdl	bdl	bdl	bdl	bdl	bdl	bdl	bdl	bdl	bdl	bdl	bdl
CaO	13.20	12.87	12.56	10.98	11.73	11.68	11.46	11.50	11.60	10.95	10.89	11.02	10.81	11.2
Na_2O	2.55	2.53	2.55	2.44	2.10	1.89	1.88	2.07	1.98	2.50	2.33	2.54	2.69	2.52
K_2O	0.11	0.08	0.08	0.06	0.12	0.13	0.11	0.13	0.09	0.05	0.03	0.06	0.04	0.04
NiO	bdl	bdl	bdl	bdl	bdl	bdl	bdl	bdl	bdl	bdl	bdl	bdl	bdl	bdl
BaO	bdl	bdl	bdl	bdl	bdl	bdl	bdl	bdl	bdl	bdl	bdl	bdl	bdl	bdl
Total	98.68	97.25	96.62	97.32	97.72	97.09	96.74	96.99	97.19	97.22	97.66	96.97	97.12	96.90
Si	6.323	6.289	6.390	6.302	6.389	6.386	6.368	6.412	6.374	6.213	6.250	6.168	6.123	6.156
Al IV	1.677	1.711	1.610	1.698	1.611	1.614	1.632	1.588	1.626	1.787	1.750	1.832	1.877	1.844
Al VI	0.855	0.549	0.435	0.484	0.199	0.195	0.177	0.253	0.179	0.485	0.511	0.608	0.598	0.681
Ti	0.056	0.065	0.065	0.009	0.237	0.276	0.277	0.246	0.272	0.007	0.004	0.005	0.005	0.004
Fe^{3+}	0.000	0.335	0.431	1.176	0.717	0.693	0.798	0.697	0.745	1.262	1.295	1.120	1.222	1.008
Fe^{2+}	0.975	0.724	0.588	0.134	0.679	0.672	0.579	0.578	0.637	0.032	0.070	0.233	0.099	0.333
Cr	0.000	0.000	0.000	0.000	0.000	0.000	0.000	0.000	0.000	0.000	0.000	0.000	0.000	0.000
Mn	0.000	0.000	0.000	0.019	0.000	0.026	0.016	0.000	0.000	0.030	0.023	0.030	0.028	0.022
Mg	3.085	3.312	3.464	3.173	3.147	3.132	3.149	3.212	3.151	3.180	3.096	3.000	3.041	2.952
Ca	2.012	1.987	1.942	1.667	1.804	1.808	1.776	1.772	1.791	1.663	1.646	1.687	1.647	1.720
Na	0.703	0.707	0.714	0.670	0.584	0.530	0.527	0.577	0.553	0.687	0.637	0.704	0.741	0.700
K	0.020	0.015	0.015	0.011	0.022	0.024	0.020	0.024	0.017	0.009	0.005	0.011	0.007	0.007
(Ca+Na) (B)	2.012	2.000	2.000	2.000	2.000	2.000	2.000	2.000	2.000	2.000	2.000	2.000	2.000	2.000
Na (B)	0.000	0.013	0.058	0.333	0.196	0.192	0.224	0.228	0.209	0.337	0.354	0.313	0.353	0.280
(Na+K) (A)	0.723	0.708	0.671	0.349	0.410	0.362	0.324	0.373	0.360	0.359	0.289	0.402	0.395	0.427
Mg#	76.0	75.8	77.3	70.8	69.3	69.7	69.6	71.6	69.5	71.1	69.4	68.9	69.7	68.8

Number of ions on the basis of 23 (O); *total Fe is expressed as FeO; bdl, below detection limit; r = rim.

composition. The Cr_2O_3 content of the clinopyroxenes vary between 0.12-0.51 wt% in olivine gabbro and 0.11-0.24 wt% in gabbro. The TiO_2 content of the clinopyroxenes is in the range 0.20-0.48 wt% in olivine gabbro and 0.14-0.73 wt% in the gabbros. The Mg number (Mg# = Mgx100/Mg + Fe_{tot}) of the clinopyroxenes ranges from 77.8 to 92.1 in olivine gabbros and from 75.0 to 87.2 in gabbros (Table 4).

Orthopyroxene

The orthopyroxenes are unzoned and are hypersthene in composition (Fig. 7a). In terms of quadrilateral components, orthopyroxene compositions are $En_{76.8\text{-}83.5}Fs_{15.7\text{-}21.5}Wo_{0.7\text{-}1.8}$ (Table 5), and Mg# ranges from 77.6 to 84.3.

Plagioclase

Representative analyses for the plagioclases in the mafic cumulates indicate anorthite contents between 76.4-93.7 mol% in olivine gabbros and 73.4-86.8 mol% in gabbros (Table 6).

Amphibole

The primary amphiboles in the olivine gabbros are represented by pargasitic hornblende (Fig. 7b). They contain 12-15.1% Al_2O_3, 0.5-0.6% TiO_2, 2.5-2.6% Na_2O and 0.1% K_2O by weight. In contrast, the amphiboles in the gabbros are secondary, derived from alteration of pyroxenes, due to interaction of gabbros with seawater-derived hydrothermal fluids and represented by mainly tschermakitic hornblende or tschermakite (Fig. 7b) and contain 10.6-15% Al_2O_3, 0-2.6% TiO_2, 1.9-2.7% Na_2O and 0-0.1% K_2O by weight. Mg# of the amphiboles ranges from 75.8 to 77.3 for olivine gabbros and from 68.8 to 71.6 for gabbros (Table 7).

WHOLE-ROCK CHEMISTRY

The major-element, trace-element and REE contents of the mafic cumulates are listed in Table 2. LOI values range from 0.9 to 5.4 wt% for the olivine gabbros and from 1.2 to 4.3 wt% for the gabbros. The highest LOI values measured in these rocks reflect variable secondary alteration, which is indicated by the presence of retrograde minerals (i.e., serpentine and amphibole) as discussed in the "Petrography and Mineral Chemistry" section.

Variations and correlations of some selected major and trace elements are presented in Fig. 8a-i. SiO_2 and Al_2O_3 show positive correlations with MgO, while TiO_2 and CaO do not show any correlation with MgO (Fig. 8a-d); Sr and Ga show negative correlation (Fig. 8e, f), whereas Ni, Co and Cr exhibit positive correlation with MgO (Fig. 8g-i).

The olivine gabbros show relatively low SiO_2 (42.46-48.07 wt%) and contain 12.86-20.43 wt% Al_2O_3, 0.45-1.39 wt% Na_2O, 51.1-292.9 ppm Sr, 7.8-11.5 ppm Ga, 59-427.6 ppm Ni (high), 29.3-69.1 ppm Co and 321.6-1067.4 ppm Cr. In contrast, the gabbros show relatively high SiO_2 (45.08-50.58 wt%) and contain 15.25-27.76 wt% Al_2O_3, 0.77-3.14 wt% Na_2O, 125.2-322 ppm Sr, 10.1-15.3 ppm Ga, 14.6-82.4 ppm Ni (low), 21.5-42.6 ppm Co and 13.7-513.2 ppm Cr (Table 2).

The chondrite-normalized REE and spider diagrams for the mafic cumulate rocks normalized to normal mid-ocean ridge basalt (N-MORB) are presented in Fig. 9. The REE concentrations of the olivine gabbros are 0.2 to 7.4 fold times that of chondritic abundance (Fig. 9a). They exhibit downwardly convex LREE patterns. The ratio Ce_N/Sm_N ranges from 0.21 to 0.50, and Ce_N/Yb_N, from 0.17 to 0.56, but one olivine gabbro sample (H30) shows slightly LREE-depleted patterns. The gabbros contain 0.42-11.76 times chondritic abundances and are characterized by variously LREE-depleted patterns and Ce_N/Sm_N that ranges from 0.21 to 0.75 and Ce_N/Yb_N from 0.19 to 0.66 (Fig. 9b). Two gabbro samples (H45 and H46) show slightly LREE-depleted patterns while others display REE patterns similar to those of the olivine gabbros. The N-MORB-normalized multi-element diagram of the mafic cumulate rocks indicates that they generally are depleted in high field strength (HFS) elements (Nb, Zr, Hf, Ti), whereas some enrichment of large-ion lithophile (LIL) elements (Rb, Ba, K, Sr) has been observed in some samples (Fig. 9c, d).

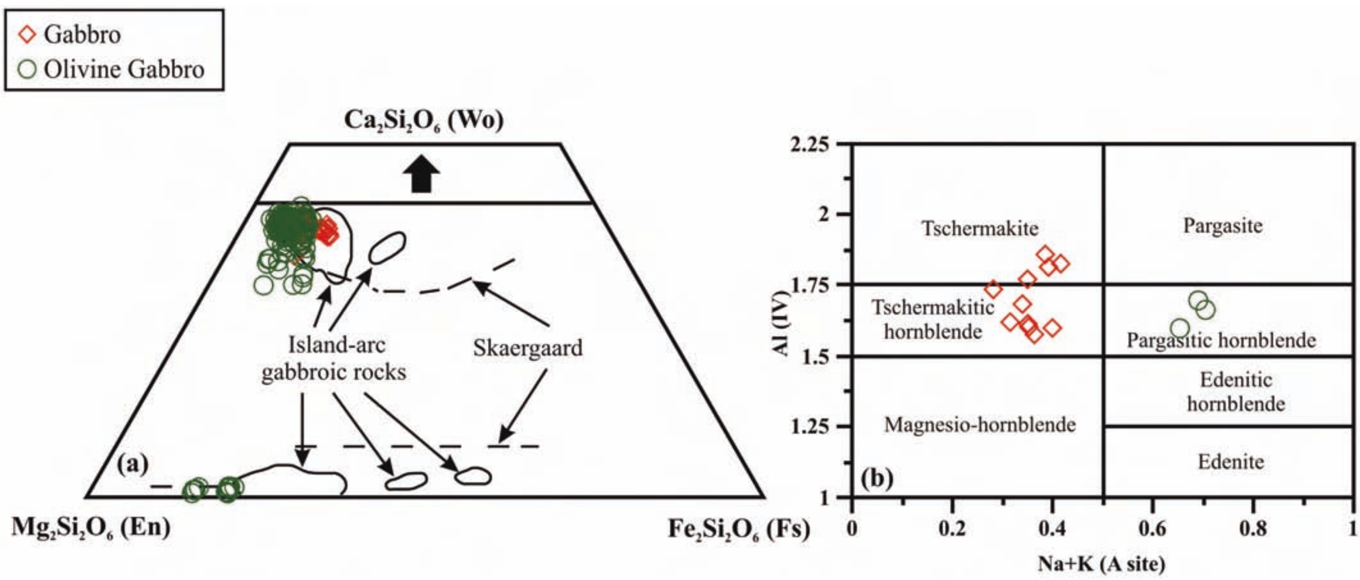

Fig. 7 - (a) Pyroxene ternary diagram showing clinopyroxene and orthopyroxene compositions from the mafic cumulate rocks (nomenclature from Morimoto et al., 1988). Fields of island arc gabbroic rocks and Skaergaard trends are from Burns (1985), (b) Plot of Al(IV) versus cations in A-site for amphibole in the cumulate gabbros (nomenclature from Leake, 1978).

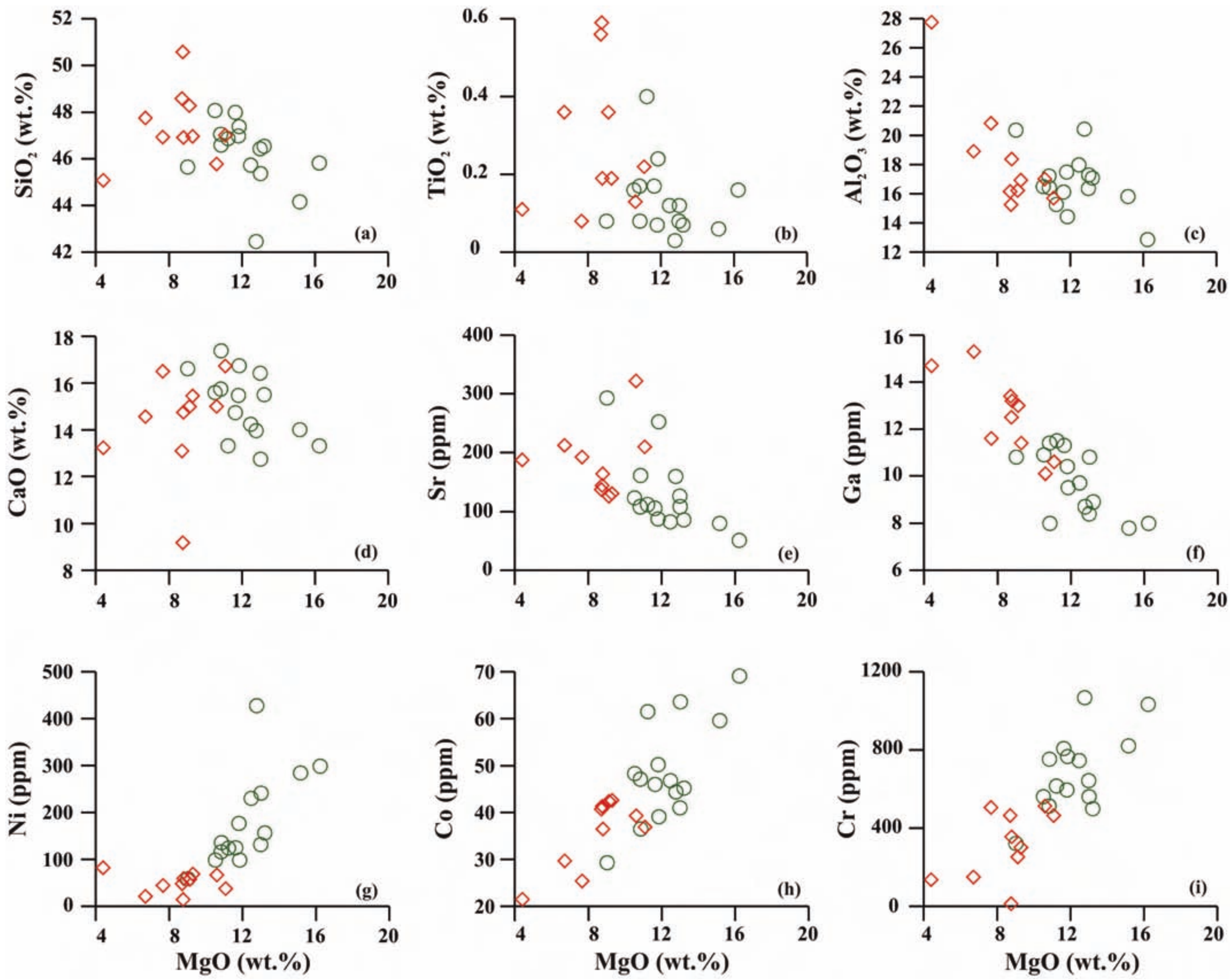

Fig. 8 - Selected major and trace element variation diagrams of the mafic cumulate rocks of the Kuluncak (Malatya) ophiolite. Symbols as in Fig. 7.

DISCUSSION

New petrologic and geochemical data obtained in the present study from the cumulates of the Kuluncak (Malatya) ophiolite suggest that mafic cumulate rocks evolved by fractional crystallization and gravitational differentiation. The mineral chemistries of olivine, orthopyroxene, clinopyroxene and plagioclase within cumulates have been used to establish the tectonic setting for cumulates of the ophiolitic sequences (Elthon et al., 1982; 1984; Komor et al., 1985; Burns, 1985; Thy, 1987; 1990; Hébert and Laurent, 1990; Parlak et al., 2000; 2002; Bağcı et al., 2005). On this basis, the petrogenesis and tectonic implications are discussed below.

Petrogenesis

The cumulates define a trend that is consistent with the progressive removal of cumulate phases, such as olivine, clinopyroxene and plagioclase, from the magma. The overall differentiation trend is from highly magnesian olivine gabbros to gabbros rich in Al_2O_3, CaO and Sr (Table 2, Fig. 8c-e). The high Al_2O_3 and CaO contents of the cumulates are evidence of crystallization of Ca-rich plagioclase (An_{73-94}) within the magma chamber of the Kuluncak ophiolite. The Sr content of the gabbroic cumulates increases notably with decreasing MgO, owing to the increasing modal plagioclase in the gabbroic cumulates (Grove and Baker, 1984; Beard, 1986). The Ga content of the cumulate rocks is negatively correlated with MgO (Fig. 8f) since the Ga is incompatible element in olivine. The compatible trace elements, such as Ni, Co and Cr, decrease from notably high values in the olivine gabbros to much lower values in the gabbros (Table 2, Fig. 8g-i), which is consistent with fractionation of olivine, spinel and clinopyroxene. The REE and multi-element patterns of the mafic cumulates exhibit slight enrichment in LIL elements and negative Nb and Zr anomalies (Fig. 9c, d). High concentrations of LIL relative to HFS elements in subduction zone magmas originate from fluids and/or siliceous melts derived from a subducting oceanic slab. These slab-derived fluids have high concentrations of LIL elements, whereas HFSE and Nb are retained in the slab (Pearce, 1982; Arculus and Powel, 1986; Yogodzinski et al., 1993; Wallin and Metcalf, 1998). The slab-derived fluid, the subducted sediment, and the overlying mantle wedge are the three main sources for the trace-element signature of subduction-related magmas (Perfit et al., 1980;

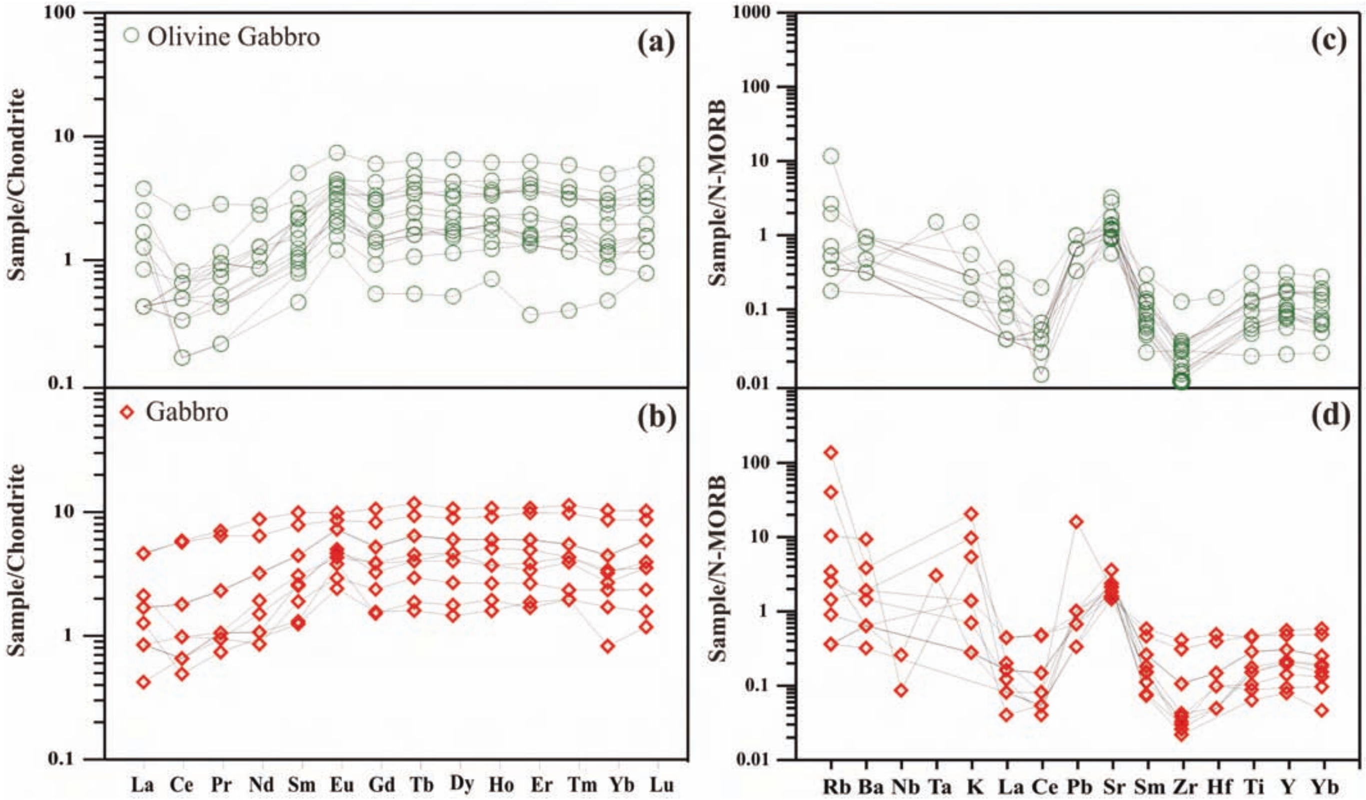

Fig. 9 - Chondrite-normalized REE (a, b) and N-MORB normalized spider (c, d) diagrams for the mafic cumulate rocks of the Kuluncak (Malatya) ophiolite (normalizing values are from Sun and McDonough, 1989).

Pearce, 1982; Arculus and Powell, 1986). The incompatible element patterns are comparable to those of the cumulate gabbros from the Kızıldağ ophiolite (Dilek and Thy, 2009), cumulate gabbros from the Neyriz ophiolite (Moghadam and Stern, 2014) and the ultramafic-mafic cumulates from the ophiolitic rocks of the southern Kahramanmaraş Province (Bağcı, 2013; Tanırlı and Rızaoğlu, 2016).

In SSZ ophiolites, clinopyroxene and sometimes orthopyroxene commonly crystallize before plagioclase (Pearce et al., 1984). Jacques and Green (1980) demonstrated that the first phase crystallizing after olivine in a cumulate series is determined by the degree of partial melting that occurred in the lherzolite mantle source region. Olivine → plagioclase corresponds to low, olivine → clinopyroxene to medium, and olivine → orthopyroxene to high degrees of partial melting. Ishiwatari (1985) demonstrated that the TiO_2 content of the clinopyroxene within these three kinds of crystallization trends may be an indicator of the next phase crystallizing after olivine: (1) plagioclase-type cumulates have high TiO_2 (0.6-0.8 wt%), (2) clinopyroxene-type cumulates have moderate TiO_2 (0.4 wt%) and (3) orthopyroxene-type cumulates have low TiO_2 (0.1 wt%). The order of crystallization in cumulates and the average TiO_2 contents of clinopyroxenes (0.20-0.48 wt% in olivine gabbros and 0.14-0.73 wt% in gabbros) from cumulates of the Kuluncak ophiolite are consistent with a parental magma being generated by a low to moderate degree of partial melting, leaving a mantle residue represented by the harzburgites.

The extremely low Ti contents of the clinopyroxenes in the cumulates of the Kuluncak ophiolite support crystallization of clinopyroxenes from a Ti-poor magma (Fig. 10a). Ti in clinopyroxenes is believed to reflect the degree of depletion of the mantle source and the Ti activity of the parent magma (Pearce and Norry, 1979). The absence of lherzolitic ultramafic rock type in the mantle tectonites and the extremely low Ti contents of the clinopyroxenes in the cumulates suggest that one or several earlier partial melting events removed the Ti from the mantle clinopyroxenes (Hébert and Laurent, 1990). Remelting of previously depleted peridotite might lead to such depletion (Duncan and Green, 1980). This magmatic process is believed to be responsible for crystallization of the Ti-poor clinopyroxenes in the cumulate rocks from the Kuluncak ophiolite. Ti-poor magma was the source for the ophiolites that formed in a SSZ setting, whereas the MORB-type ophiolites are characterized by relatively high Ti contents. Low Ti contents have been reported for clinopyroxenes in Eastern Mediterranean ophiolitic basalts and plutonic rocks, including the Pindos and Troodos ophiolites (Capedri and Venturelli, 1979), Oman ophiolite (Pallister and Hopson 1981), Bay of Islands ophiolite complex (Malpas, 1978), Sarıkaraman ophiolite (Yalınız and Göncüoğlu, 1999), Pozantı-Karsantı ophiolite (Parlak et al., 2000; 2002), Kızıldağ ophiolite (Bağcı et al., 2005), Tekirova ophiolite (Bağcı et al., 2006) and the ophiolitic rocks from the southern Kahramanmaraş Province (Bağcı, 2013; Tanırlı and Rızaoğlu, 2016).

The Cr_2O_3 content of cumulate clinopyroxenes decreases with their decreasing Mg#, a correlation that may be related to gradual Cr impoverishment of the magma with differentiation (Hodges and Papike, 1976). This correlation is plotted in Fig. 10b. Most of the clinopyroxenes in the gabbros and some clinopyroxenes in the olivine gabbros that have relatively lower Mg# overlap with the field of low-pressure clinopyroxenes of N-MORB (Elthon, 1987), whereas most of the clinopyroxenes in the olivine gabbros and some clinopyroxenes have relatively higher Mg# and plot outside

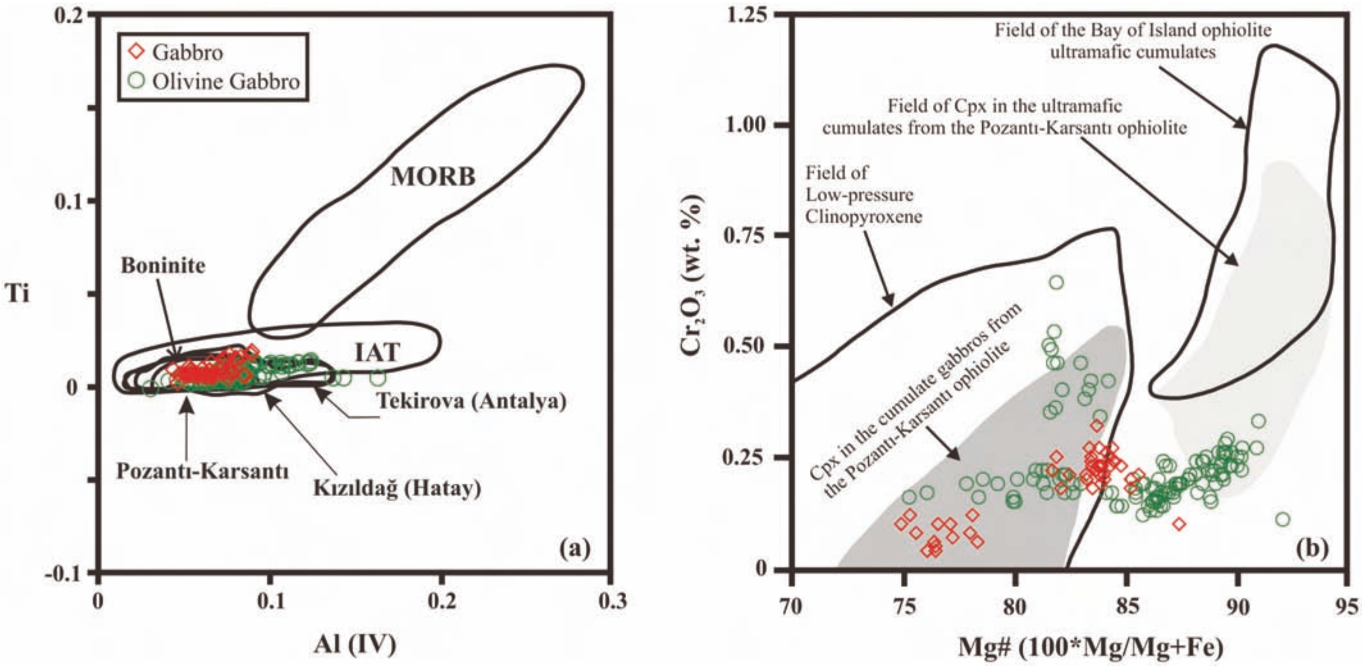

Fig. 10 - (a) Covariation of Ti versus Al (IV) diagram for the clinopyroxenes from the mafic cumulate rocks. Fields of MORB, IAT and boninite are from Beccaluva et al. (1989). Fields for the Pozantı-Karsantı ophiolite are from Parlak et al. (2000; 2002), Kızıldağ (Hatay) and Tekirova (Antalya) ophiolites are from Bağcı (2004), (b) Cr_2O_3 versus Mg number in clinopyroxenes of the mafic cumulate rocks. Low-pressure Cpx field is from 1-atm experimental studies of N-MORB (Elthon, 1987). Field of Bay of Island ophiolite complex ultramafic cumulates is from Elthon (1987). Field of clinopyroxenes in the ultramafic and mafic cumulates of the Pozantı-Karsantı ophiolite is from Parlak et al. (2000; 2002).

the field of low-pressure clinopyroxenes of N-MORB. This different trend implies that mafic cumulates of the Kuluncak ophiolite formed under low to moderate-pressure conditions and are similar to those of the Pozantı-Karsantı ophiolite (Parlak et al., 2000), the Bay of Island ophiolite complex (Elthon et al., 1982; 1984), Troodos ophiolite (Hébert and Laurent, 1990), Mersin ophiolite (Parlak et al., 1996) and Tekirova and Kızıldağ ophiolites (Bağcı, 2004).

The presence of high An-content plagioclases in gabbroic rocks from island arcs (Jaques, 1981; Dupuy et al., 1982; Beard, 1986; Fujimaki, 1986; DeBari et al., 1987; DeBari and Coleman, 1989; Thy et al., 1989), and has been ascribed to the presence of H_2O in the melt during crystallization (Helz, 1973). Experimental data on the crystallization of highly calcic plagioclases in cumulates indicate that primary magmas with high (> 13) CaO/Na_2O ratios (Jaques, 1981) or basaltic melts with low CaO/Na_2O ratios (< 7) and high water pressure (2-6%) (Sisson and Grove, 1993). The high-Ca plagioclases in the mafic cumulate rocks have been widely reported in cumulate rocks from many supra-subduction zone-type ophiolites in the Eastern Mediterranean region (Parlak et al., 1996; 2000; Hébert and Laurent, 1990; Bağcı et al., 2005; 2006; Sarıfakıoğlu et al., 2009; Bağcı, 2013). Pargasitic amphiboles also occur in gabbroic rocks in subduction-related tectonic environments, such as island arc (Beard, 1986; Tiepolo and Tribuzio, 2005), back-arc (Harigane et al., 2011) and ophiolitic settings (Tribuzio et al., 2000). The origin of pargasitic amphiboles, for some workers have proposed that it is of igneous origin (Gillis, 1996; Tribuzio et al., 2000; Gillis and Meyer, 2001; Coogan et al., 2001) whereas others have argued for an origin hydrotermal which resulting from reactions between igneous minerals and oceanic fluids (Campbell et al., 1988; Michard, 1989; Gillis and Meyer, 2001). The pargasitic amphibole was the final major phase to crystallize in gabbroic rocks from Argentine and Alaskan lower crustal suites (Debari, 1997), as a results of the reaction between the pyroxene and melt. This reaction is reported melting experiments on hydrous basaltic composition (Helz 1973; Holloway and Burnham, 1972). The presence of the pargasitic amphibole and An-rich plagioclase in the cumulate gabbros of the Kuluncak ophiolite indicates that they were derived from a tholeiitic magma in an intra-oceanic subduction-related setting where the melting of the mantle wedge was facilitated by the addition of volatiles from the subducting slab.

The Fe-Mg partition for the olivine-clinopyroxene pairs is plotted in Fig. 11. The Fe-Mg distribution suggests that olivines are chemically in equilibrium with clinopyroxenes at a subsolidus state (Mori and Banno, 1973). The olivines and clinopyroxenes are unzoned in the gabbroic cumulates of the Kuluncak ophiolite. The olivine-clinopyroxene pairs indicate high equilibration temperatures, above 700°C (Obata et al., 1974), for the gabbroic cumulates in the Kuluncak ophiolite. The crystallization conditions of the cumulate rocks were determined by several methods and calculations (Brey and Köhler, 1990; Taylor, 1998). For olivine gabbros from the cumulate rocks of the Kuluncak ophiolite, the two-pyroxene thermometer of Brey and Köhler (1990) yielded temperatures of 834-936°C (Table 8). The two-pyroxene geo-thermo-barometer (Putirka, 2008) was used for estimating the temperatures and pressures of crystallization of the olivine gabbros. This method yielded temperatures of 929-943°C in equation 36 and 884-913°C in equation 37 and pressures of 3.4-4.8 kbar for these rocks (Table 8). These moderate pressure estimates suggest a depth of 10-15 km for the crystallization of the olivine gabbros in the cumulate rocks of the Kuluncak ophiolite. This implies that the cumulate gabbros were derived from the root of a nascent island arc setting during Late Cretaceous.

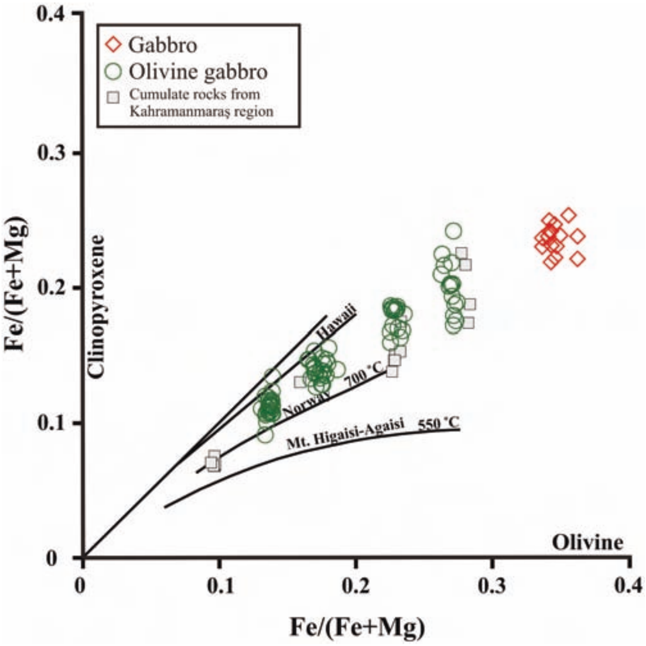

Fig. 11 - Mg-Fe partition relations between olivine and clinopyroxene. Isotherms (700°C and 550°C) are from Obata et al. (1974). Ultramafic-mafic cumulates of the ophiolitic rocks of the southern Kahramanmaraş region from Bağcı (2013).

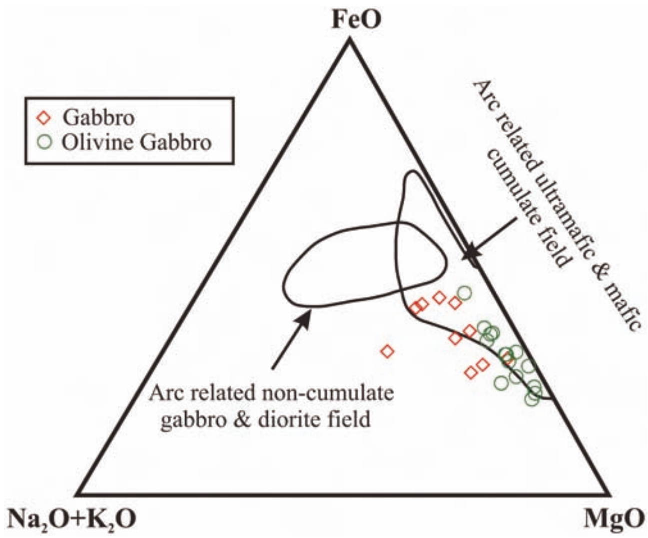

Fig. 12 - AFM compositions of the mafic cumulate rocks. Fields of cumulate and non-cumulate rocks are from Beard (1986).

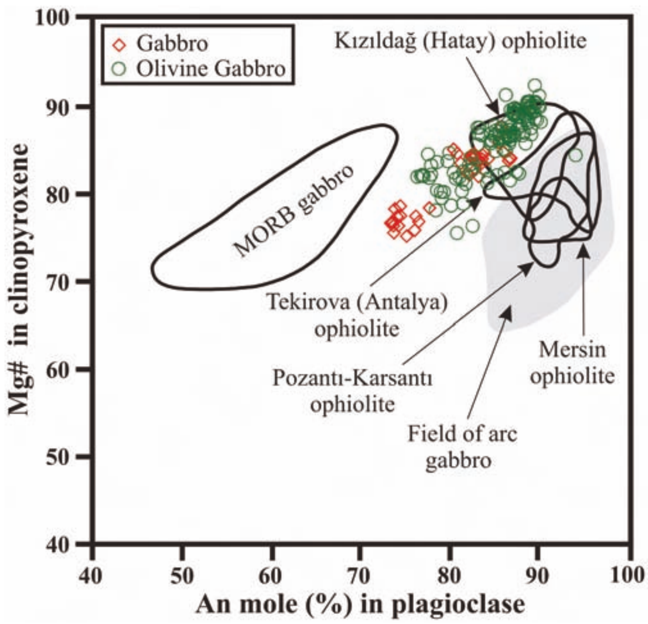

Fig. 13 - Composition of coexisting plagioclase (An mol%) and clinopyroxene (Mg-number) in the mafic cumulate rocks. Fields of MORB and arc gabbro are from Burns (1985). Fields for the Mersin and Pozantı-Karsantı ophiolites are from Parlak et al. (1996; 2000), the Kızıldağ (Hatay) and Tekirova (Antalya) ophiolites are from Bağcı et al. (2005; 2006).

Tectonic implications

In the AFM diagram (Beard, 1986), the mafic cumulates under investigation (Fig. 12) show enrichment from MgO toward FeO. The composition of mafic cumulate rocks is consistent with their formation in an arc-related tectonic environment.

Burns (1985) reported that the iron-rich pyroxene ($Fs_{6-13}En_{45-40}En_{81-63}$) coexisting with calcic plagioclase (An_{75-100}) in the gabbroic rocks of the Border Ranges ultramafic-mafic complex (BRUMC) and their association with magnetite are common in plutonic xenoliths in island-arc rocks. Covariation of the Mg# in clinopyroxene with the An content of the plagioclase from the mafic cumulates is shown in Fig. 13, which shows that the cumulate samples that plot within the field of arc-related gabbros differ from those of gabbros formed at mid-ocean ridge setting and resemble gabbroic rocks from the ophiolites of Mersin (Parlak et al., 1996), Pozantı-Karsantı (Parlak et al., 2000), Kızıldağ (Hatay) (Bağcı et al., 2005) and Tekirova (Antalya) (Bağcı et al., 2006).

Table 8 - Estimated temperatures (T) and pressures (P) for the olivine gabbros from the cumulate rocks.

	Brey and Kohler (1990)	Putirka (2008)				Observed
	T(BKN)	Eqn 36	Eqn 37	Eqn 38	Eqn 39	K_D(Fe-Mg)
Sample	T(C)	T(C)	T(C)	P(kbar)	P(kbar)	
H-13	906	943	913	3.6	3.5	0.84
H-15	834	929	884	4.8	3.4	0.81

Test for Equilibrium: (K_D should be 1.09±.14); Equation 39 uses equation 36 for the temperature input.

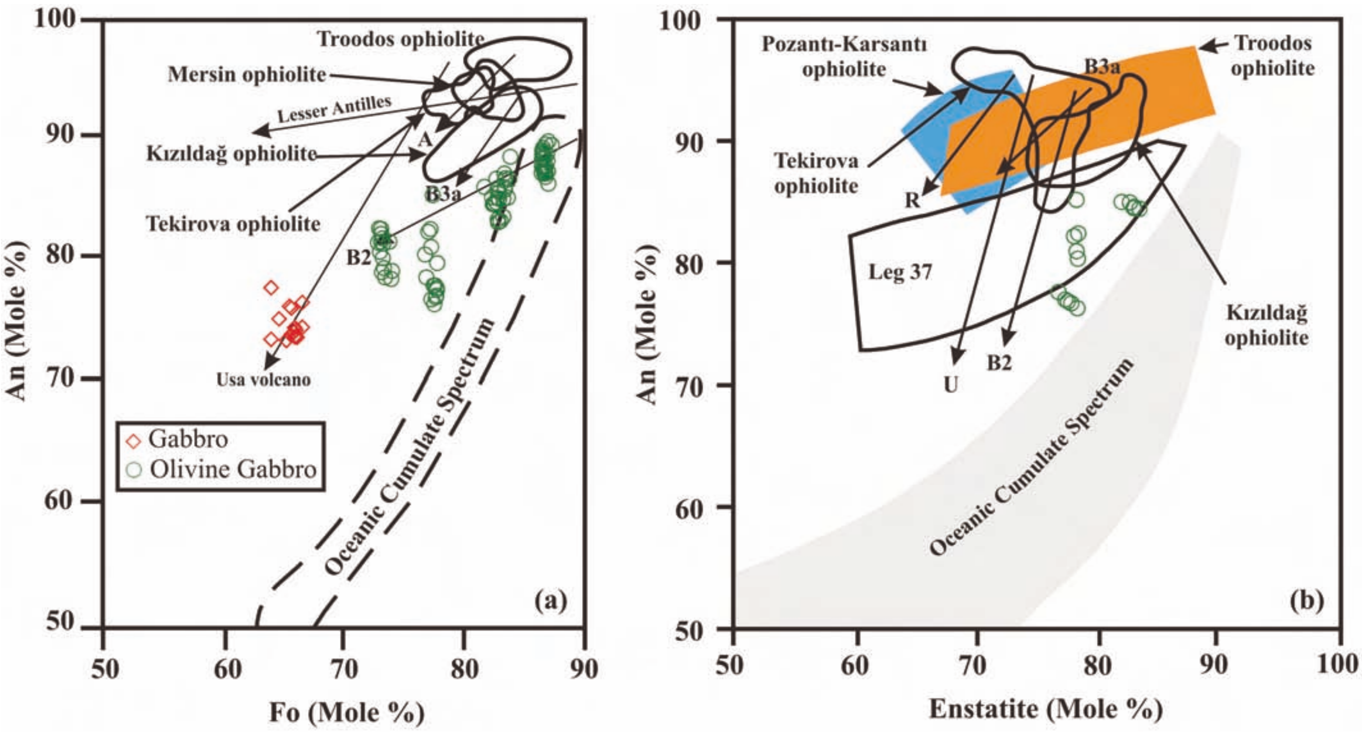

Fig. 14 - (a) Anorthite content in plagioclase (mol%) versus Fo (mol%) content in olivine, (b) Anorthite content in plagioclase (mol%) versus enstatite content in orthopyroxene (mol%) for the Kuluncak (Malatya) ophiolite. The Troodos ophiolite trend is from Hébert and Laurent (1990). The Mersin ophiolite trend is from Parlak et al. (1996). The Pozantı-Karsantı ophiolite trend is from Parlak et al. (2000). The Kızıldağ ophiolite trend is from Bağcı et al. (2005). The Tekirova ophiolite trend is from Bağcı et al. (2006). R- Rindjami Volcano (Foden, 1983); B2- B3a- Boisa Volcano (Gust and Johnson, 1981); U- Usa Volcano (Fujimaki, 1986); A- Agrigan Volcano (Stern, 1979); Lesser Antilles is from Arculus and Wills (1980). The oceanic cumulate spectrum is from Hébert and Laurent (1990).

Plots of the covariation of the An content of plagioclase with the Fo content of olivine and the En content of orthopyroxenes in cumulate rocks are presented in Fig. 14 together with some Eastern Mediterranean ophiolites and other well-documented tectonic settings. The mineral composition of the Kuluncak ophiolite cumulates indicates very limited fractionation and differs from compositions characteristic of mid-ocean ridge oceanic cumulates. On the other hand, they display compositions similar to cumulates from the Eastern Mediterranean ophiolites (Hébert and Laurent, 1990; Parlak et al., 1996; 2000; Bağcı et al., 2005; 2006) and from island-arc systems (Stern, 1979; Arculus and Wills, 1980; Gust and Johnson, 1981; Fujimaki, 1986). The high An contents of the plagioclases indicate that the cumulates of the Kuluncak ophiolite did not crystallize under low-pressure anhydrous conditions. Experimental studies show that the effect of increasing pressure under anhydrous conditions results in a decrease in the An content of plagioclase coexisting with olivine (Green, 1969; Bender et al., 1978). The effect of high PH_2O on the equilibrium plagioclase compositions in simplified systems is known to be an increase in the An content (Yoder, 1969; Johannes, 1978; Takagi et al., 2005; Hamada and Fujii, 2007). The crystallization of the high-An plagioclase found in some island-arc lavas requires PH_2O and temperatures that exceed reasonable estimates (Arculus and Wills, 1980; Gill, 1981). Arculus and Wills (1980) proposed that the addition of another phase to the plagioclase-water system (e.g., quartz, diopside or amphibole) would drastically lower equilibrium temperatures and steepen the high An part of the solidus of the plagioclase melting loop.

The geological history of the Mediterranean region was dominated by the opening of the Neotethys Ocean, mainly during the Early Mesozoic (Robertson and Comas, 1998). During the Triassic Period, one or several microcontinents rifted from Gondwana and drifted northwards, thereby opening a Mesozoic ocean basin (Şengör and Yılmaz, 1981; Robertson and Dixon, 1984). At the end of the Early Cretaceous Period, depending on the opening of the South Atlantic Ocean, the divergent regime passed through the convergent regime in the Neotethys oceanic basin between the Eurasian and African plates (Livermore and Smith, 1984; Savostin et al., 1986; Dilek et al., 1999). In this compressive regime, northward subduction lead to SSZ ophiolites within several oceanic basins, namely, the İzmir-Ankara-Erzincan, the Inner Tauride and the Southern Neotethys (Şengör and Yılmaz, 1981; Robertson and Dixon, 1984; Görür et al., 1984; Dilek et al., 1999; Robertson et al., 2012) (Fig. 15). The Kuluncak ophiolite is in the Tauride belt in the eastern part of Central Anatolia. Based on ophiolite classification (Pearce et al., 1984; Shervais, 2001; Robertson, 2002; Pearce, 2003; Saccani and Photiades, 2004; Arai et al., 2006; Pearce, 2008; Pearce and Robinson, 2010; Dilek and Furnes, 2011) and several tectonic models of the Eastern Tauride region (Perinçek and Kozlu, 1984; Gürer, 1994; Parlak et al., 2006; Robertson et al., 2012; 2013), our results indicate that the Kuluncak ophiolites were formed in an intra-oceanic subduction zone during the closure of the Inner Tauride Ocean in Late Cretaceous and emplaced over the Tauride carbonate platform. After the emplacement of the Kuluncak ophiolite onto a passive continental margin, the Hekimhan Basin (supra-

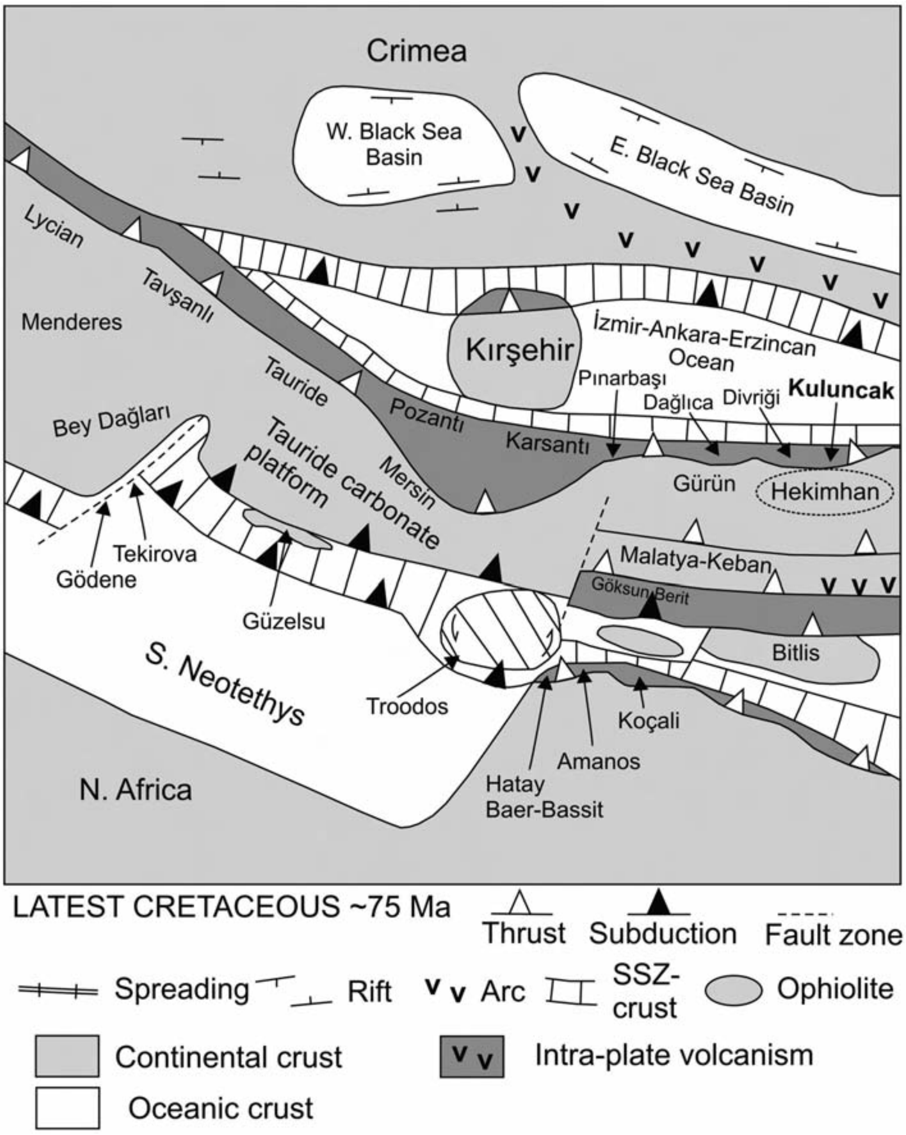

Fig. 15 - Regional palaeotectonic reconstructions of the Eastern Mediterranean region during the Late Cretaceous (modified from Robertson et al., 2012; Booth et al., 2014).

ophiolite basin) formed as part of the northern margin of the Tauride microcontinent during the collision and suturing of the Inner Tauride Ocean and the İzmir-Ankara-Erzincan Ocean (Booth et al., 2014).

CONCLUSIONS

Based on the field observation, petrological and geochemical studies on mafic cumulates from the Kuluncak ophiolite, the main conclusions are as follows:

1. Mafic cumulate rocks from the Kuluncak ophiolite are composed of olivine gabbro and gabbro. The crystallization order for the cumulate rocks is olivine → plagioclase → clinopyroxene → orthopyroxene → amphibole.
2. Major and trace element geochemistry as well as the mineral chemistry of the mafic cumulates indicate these rocks were derived from an island arc tholeiitic (IAT) magma and resemble those of island arc suites and the Eastern Mediterranean ophiolites.
3. The mineral chemistry of the cumulates suggests a low- to moderate pressure conditions for the mafic cumulates during the magma fractionation and magma chamber evolution of the Kuluncak ophiolite.
4. The Kuluncak ophiolite was emplaced southwards onto the northern edge of the Tauride-Anatolide continent during latest Cretaceous time.

ACKNOWLEDGMENTS

This article was derived from a master of science thesis of Murat Camuzcuoğlu. This study was supported by the Research Fund of Mersin University in Turkey with Project Number BAP-FBE JM (MC) 2011-2 YL. We are very grateful to Eugenio Piluso and Paola Tartarotti for their constructive and very helpful comments. We also thank Osman Parlak for valuable comments and suggestions. Yüksel Metin and Hayati Koç are thanked for fruitful discussions on the regional geology of the study area. We would like to thank Alessandra Montanini for her efforts during editorial handling.

REFERENCES

Arai S., Kadoshima K. and Morishita T., 2006. Widespread arc-related melting in the mantle section of the northern Oman ophiolite as inferred from detrital chromian spinels. J. Geol. Soc. London, 163: 1-11.

Arculus R.J. and Powell R., 1986. Source component mixing in the regions of arc magma generation. J. Geophys. Res., 91: 5913-5926.

Arculus R.J. and Wills K.J.A., 1980. The petrology of plutonic blocks and inclusions from Lesser Antilles island arc. J. Petrol., 21: 743-799.

Bağcı U., 2004. Geochemistry and petrology of the Kızıldağ (Hatay) and Tekirova (Antalya) Ophiolites. Çukurova Univ., Ph.D. Thesis, 383 pp. (unpublished) (in Turkish with English abstract).

Bağcı U., 2013. The geochemistry and petrology of the ophiolitic rocks from the Kahramanmaraş region, Southern Turkey. Turk. J. Earth Sci., 22: 536-562.

Bağcı U. and Parlak O., 2009. Petrology of the Tekirova (Antalya) ophiolite (Southern Turkey): Evidence for diverse magma generations and their tectonic implications during Neotethyan-subduction. Int. J. Earth Sci., 98: 387-405.

Bağcı U., Parlak O. and Höck V., 2005. Whole rock and mineral chemistry of cumulates from the Kızıldağ (Hatay) ophiolite (Turkey): clues for multiple magma generation during crustal accretion in the southern Neotethyan Ocean. Miner. Mag., 69: 39-62.

Bağcı U., Parlak O. and Höck V., 2006. Geochemical character and tectonic environment of ultramafic to mafic cumulates from the Tekirova (Antalya) ophiolite (southern Turkey). Geol. J., 41: 193-219.

Bağcı U., Parlak O. and Höck V., 2008. Geochemistry and tectonic environment of diverse magma generations forming the crustal units of the Kızıldağ (Hatay) ophiolite, Southern Turkey. Turk. J. Earth Sci., 17: 43-71.

Beard J.S., 1986. Characteristic mineralogy of arc-related cumulate gabbros: implications for the tectonic setting of gabbroic plutons and for andesite genesis. Geology, 14: 848-851.

Beccaluva L., Macciotta G., Piccardo G.B. and Zeda O., 1989. Clinopyroxene composition of ophiolite basalts as petrogenetic indicator. Chem. Geol., 77: 165-182.

Bender J.F., Hodges F.N. and Bence A.E., 1978. Petrogenesis of basalts from the project FAMOUS area: experimental study from 0 to 15 kbar. Earth Planet. Sci. Lett., 41: 277-302.

Beyarslan M. and Bingöl A.F., 2000. Petrology of a supra-subduction zone ophiolite (Elazığ, Turkey). Can. J. Earth Sci., 37: 1411-1424.

Booth M.G., Robertson A.H.F., Taslı K. and İnan N., 2014. Late Cretaceous to Late Eocene Hekimhan Basin (Central Eastern Turkey) as a supra-ophiolite sedimentary/magmatic basin related to the later stages of closure of Neotethys. Tectonophysics, 635: 6-32.

Brey G.P. and Köhler T., 1990. Geothermometry in four-phase lherzolites II. J. Petrol., 31: 1353-1378.

Burns L.E., 1985. The Border Ranges ultramafic and mafic complex, south central Alaska: cumulate fractionates of island arc volcanics. Can. J. Earth Sci., 22: 1020-1038.

Campbell A.C., Palmer M.R., Kinkhammer G.P., Bowers T.S., Edmond J.M., Lawrence J.R., Casey J.F., Thompson G., Humpris S., Rona P. and Karson J.A., 1988. Chemistry of hot springs on the Mid-Atlantic Ridge. Nature, 335: 514-519.

Camuzcuoğlu M., 2012. The petrography and geochemistry of cumulates from ophiolitic rocks in Hekimhan (Malatya) Region. Mersin Univ., M.Sci., Thesis, 104 pp. (unpublished) (in Turkish with English abstract).

Camuzcuoğlu M. and Bağcı U., 2016. The geochemistry of rodingites in the Kuluncak (Malatya) ophiolite, SE Turkey. 7th Geochem. Symp. with Intern. participation, Antalya. Abstr., p. 286.

Camuzcuoğlu M., Bağcı U., Koepke J. and Wollf P.E., 2013. Geochemical characteristics and tectonic significance of mafic cumulates in Kuluncak ophiolite (Malatya), SE Turkey. Goldschmidt 2013, J. Conf. Abstr., p. 816.

Capedri S. and Venturelli G., 1979. Clinopyroxene composition of ophiolitic metabasalts in the Mediterranean area. Earth Planet. Sci. Lett., 43: 61-73.

Coogan L.A., Wilson R.N., Gillis K.M. and MacLeod C.J., 2001. Near-solidus evolution of oceanic gabbros: insights from amphibole geochemistry. Geochim. Cosmochim. Acta, 65: 4339-4357.

Dare S.A.S., Pearce J.A., Mcdonald I. and Styles M.T., 2009. Tectonic discrimination of peridotites using fO_2-Cr# and Ga-Ti-Fe^{III} systematic in chrome-spinel. Chem. Geol., 261: 199-216.

DeBari S.M., 1997. Evolution of magmas in continental and oceanic crust; the role of the lower crust, Can. Mineral., 35: 501-515.

DeBari S.M. and Coleman R.G., 1989. Examination of the deep levels of an island arc: evidence from the Tonsina ultramafic-mafic assemblage, Tonsina, Alaska. J. Geophys. Res., 94: 4373-4391.

DeBari S., Kay S.M. and Kay R.W., 1987. Ultramafic xenoliths from Adagdak volcano, Adak, Aleutian islands, Alaska: deformed igneous cumulates from the Moho of an island arc. J. Geol., 95: 329-341.

Dilek Y. and Flower M.F.J., 2003. Arc-trench rollback and forearc accretion: 2. A model template for ophiolites in Albania, Cyprus, and Oman. In: Y. Dilek and P.T. Robinson (Eds.), Ophiolites in Earth history. Geol. Soc. London Spec. Publ., 218: 43-68.

Dilek Y. and Furnes H., 2011. Ophiolite genesis and global tectonics: Geochemical and tectonic fingerprinting of ancient oceanic lithosphere. Geol. Soc. Am. Bull., 123: 387-411.

Dilek Y. and Moores E.M., 1990. Regional tectonics of the Eastern Mediterranean ophiolites. In: J. Malpas, E. Moores, A. Panayiotou and C. Xenophontos (Eds.), Proceed. Troodos Ophiolite Symp.,Cyprus, p. 295-309.

Dilek Y. and Thy P., 2009. Island arc tholeiite to boninitic melt evolution of the Cretaceous Kızıldağ (Turkey) ophiolite: Model for multi-stage early arc-forearc magmatism in Tethyan subduction factories. Lithos, 113: 68-87.

Dilek Y., Thy P., Hacker B. and Grundvig S., 1999. Structure and petrology of Tauride ophiolites and mafic dyke intrusions (Turkey): implications for the Neotethyan Ocean. Geol. Soc. Am. Bull., 111: 1192-1216.

Duncan R.A. and Green D.H., 1980. Role of multi-stage melting in the formation of oceanic crust. Geology, 8: 22-26.

Dupuy C., Dostal J., Marcelot G., Bougault H., Joron J.L. and Treuil M., 1982. Geochemistry of basalt from central and southern New Hebrides arc: Implications for their source rock composition. Earth Planet Sci. Lett., 60: 207-225.

Elthon D., 1987. Olivine-liquid partitioning in high-MgO basalt and komatites. 18th Lunar and Planetary Science Conference, Abstr., p. 258-259.

Elthon D., Casey J.F. and Komor S., 1982. Mineral chemistry of ultramafic cumulates from the North Arm Mountain Massif of the Bay of Islands ophiolite: Evidence for high-pressure crystal fractionation of oceanic basalts. J. Geophys. Res., 87 (B10): 8717-8734.

Elthon D., Casey J.F. and Komor S., 1984. Cryptic mineral chemistry variations in a detailed traverse through the cumulate ultramafic rocks of the North Arm Mountain massif of the Bay of Island ophiolite, Newfoundland. In: I.G. Gass, S.J. Lippard and A.W. Shelton (Eds.), Ophiolites and oceanic lithosphere. Blackwell, London, 413 pp.

Foden J.D., 1983. The petrology of calcalkaline lavas of Rindjani volcano, East Sunda Arc: Model for island arcs. J. Petrol., 24: 98-130.

Fujimaki H., 1986**.** Fractional crystallization of the basaltic suite of Usa volcano, southwest Hokkaido, Japan, and its relationships with the associated felsic suite. Lithos, 19: 129-140.

Gill J.B., 1981. Orogenic andesites and plate tectonics. Springer-Verlag, Berlin, 390 pp.

Gillis K.M., 1996. Rare earth element constraints on the origin of amphibole in gabbroic rock from site 894, Hess Deep. In: C. Mevel, K.M. Gillis, J.F. Allan and P.S. Meyer (Eds.), O.D.P. Sci. Res., 147: 59-75.

Gillis K.M. and Meyer P.S., 2001. Metasomatism of oceanic gabbros by late stage melts and hydrothermal fluids: evidence from the rare earth element composition of amphiboles. Geochem. Geophys. Geosyst., 2: 1525-2027.

Green T.H., 1969. High pressure experimental studies on the origin of anorthosite. Can. J. Earth Sci., 6: 427-440.

Grove T.L. and Baker M.B., 1984. Phase equilibrium controls on the tholeiitic versus calc-alkaline differentiation trends. J. Geophys. Res., 89: 3253-3274.

Görür N., Oktay F.Y., Seymen İ. and Şengör A.M.C., 1984. Paleotectonic evolution of the Tuzgölü basin complex, Central Anatolia: sedimentary record of a Neo-Tethyan closure. In: J.E. Dixon and A.H.F. Robertson (Eds.), The geological evolution of the Eastern Mediterranean. Geol. Soc. London Spec. Publ., 17: 455-466.

Gust D.A. and Johnson R.W., 1981. Amphibole bearing cumulates from Boisa Island, Papua New Guinea: evalution of the role of fractional crystallization in an andesitic volcano. J. Geol., 89: 219-232.

Gürer Ö.F., 1992. Geological study of Hekimhan-Hasançelebi (Malatya) region. İstanbul Univ., Ph.D. Thesis, 340 pp. (unpublished) (in Turkish with English abstract).

Gürer Ö.F., 1994. Upper Cretaceous statigraphy of Hekimhan-Hasançelebi region and the basin evolution. Geol. Bull. Turkey, 37 (2): 135-148.

Hamada M. and Fujii T., 2007. H_2O-rich island arc low-K tholeiite magma inferred from Ca-rich plagioclase-melt inclusion equilibria. Geochem. J., 41: 437-461.

Harigane Y., Michibayashi K. and Ohara Y., 2011. Deformation and hydrothermal metamorphism of gabbroic rocks within the Godzilla Megamullion, Parece Vela Basin, Philippine Sea. Lithos, 124: 185-199.

Hébert R. and Laurent R., 1990. Mineral chemistry of the plutonic section of the Troodos ophiolite: New constraints for genesis of arc-related ophiolites. In: J. Malpas, E. Moores, A. Panayiotou and C. Xenophontos (Eds.), Proceed. Troodos Ophiolite Symp. Cyprus, p. 149-163.

Helz R.T., 1973. Phase relations of basalt in their melting range at P_{H2O} = 5 kb as a function of oxygen fugacity. I. mafic phases. J. Petrol., 14: 249-302.

Hodges F.N. and Papike J.J., 1976. DSDP site 334. Magmatic cumulates from ocean layer 3, Mid Atlantic Ridge. J. Geophys. Res., 81: 4135-4151.

Holloway J.R. and Burnham C.W., 1972. Melting relations of basalt with equilibrium water pressure less than total pressure J. Petrol, 13: 1-29.

İlbeyli N., 2008. Geochemical characteristics of the Şebinkarahisar granitoids in the eastern Pontides, northeast Turkey: petrogenesis and tectonic implications. Int. Geol. Rev., 50: 563-582.

Ishiwatari A., 1985. Igneous petrogenesis of the Yakuno ophiolite (Japan) in the context of the diversity of ophiolites. Contrib. Miner. Petrol., 89: 155-167.

Jaques A.L., 1981. Petrology and petrogenesis of cumulate peridotite and gabbro from the Marum ophiolite complex, northern Papau-New Guinea. J. Petrol., 22: 1-40.

Jacques A.L. and Green D.H., 1980. Anhydrous melting of peridotite at 0-15 kb pressure and the genesis of tholeiitic basalts. Contrib. Miner. Petrol., 73: 287-310.

Johannes W., 1978. Melting of plagioclase in the system Ab-An-H_2O and Qz-Ab-An-H_2O at P_{H2O} = 5 kbars, an equilibrium problem. Contrib. Miner. Petrol., 66: 295-303.

Juteau T. and Whitechurch H., 1980. Magmatic cumulates of Antalya (Turkey): evidence of multiple intrusions in an ophiolite magma chamber. In: A. Panayiotou (Ed.), Ophiolites. Proceed. Intern. Ophiolite Symp., Geol. Survey Cyprus, p. 377-391.

Komor S.C., Elthon D. and Casey J.F., 1985. Mineralogical variations in layered ultramafic cumulate sequences at the North Arm Mountain massif, Bay of Island ophiolite, Newfoundland. J. Geophys. Res., 90: 7705-7736.

Leake B.E., 1978. Nomenclature of amphiboles. Am. Miner., 63: 1023-1052.

Livermore R.A. and Smith A.G., 1984. Some boundary conditions for the evolution of the Mediterrannean Region. In: D.J. Stanley and F.C. Wezel (Eds.), Geological evolution of the Mediterranean Basin. Springer-Verlag, Berlin, p. 83-100.

Malpas J., 1978. Magma generation in the upper mantle, field evidence from ophiolite suites and application to the generation of oceanic lithosphere. Phil. Trans. Royal Soc. London, A288: 527-546.

Metin Y., Öcal H., Çobankaya M., Tunçdemir V., Bağcı U., Uçar L., Çörekçioğlu E., Taptık M.A., Duygu L., Duran S., Rızaoğlu T. and Sevimli U.İ., 2013. Geodynamic evolution of the northern part of the Eastern Taurus (Hekimhan-Darende-Kuluncak). General Dir. Miner. Res. Explor., Report, no: 11685 (in Turkish).

Michard A., 1989. Rare earth element systematics in hydrothermal fluids. Geochim. Cosmochim. Acta, 53: 745-750.

Moghadam H.S. and Stern R.J., 2014. Ophiolites of Iran: keys to understanding the tectonic evolution of SW Asia: (I) Paleozoic ophiolites. J. Asian Earth Sci., 91: 19-38.

Mori T. and Banno S., 1973. Petrology of peridotite and garnet clinopyroxenite of the Mt. Higashi-Akaishi mass, Central Shikoku, Japan - Subsolidus relation of anhydrous phases. Contrib. Miner. Petrol., 41: 301-323.

Morimoto N., Fabries J., Ferguson A.K., Ginzburg I.V., Ross M., Seifert F.A., Zussman J., Aoki K. and Gottardi D., 1988. Nomenclature of pyroxenes. Am. Miner., 62: 53-62.

M.T.A., 2002. 1/500 000 Scale Geological Map of Turkey. General Dir. Miner Res. Explor., Ankara.

Niu Y., 2004. Bulk-rock Major and Trace Element compositions of abyssal peridotites: Implications for mantle melting, Melt extraction and post-melting processes beneath mid-ocean ridges. J. Petrol., 45: 2423-2458.

Obata M., Banno S. and Mori T., 1974. The iron-magnesium partitioning between naturally occurring coexisting olivine and Ca-rich clinopyroxene: an application of the simple mixture model to olivine solid solution. Bull. Soc. Fran. Miner. Crist., 97: 101-107.

Pallister J.S. and Hopson C.A., 1981. Samail Ophiolite plutonic suite: Field relations, phase variation, cryptic variation and layering, and a model of a spreading ridge magma chamber. J. Geophys. Res., 86 (B4): 2593-2644.

Parlak O., Delaloye M. and Bingöl E., 1996. Mineral chemistry of ultramafic and mafic cumulates as an indicator of the arc-related origin of the Mersin ophiolite (southern Turkey). Geol. Rundsch., 85: 647-661.

Parlak O., Höck V. and Delaloye M., 2000. Supra-subduction zone origin of the Pozantı-Karsantı ophiolite (southern Turkey) deduced from whole-rock and mineral chemistry of the gabbroic cumulates. In: E. Bozkurt, J.A. Winchester and J.D.A. Piper (Eds.), Tectonics and magmatism in Turkey and the surroundings area. Geol. Soc. London Spec. Publ., 173: 219-234.

Parlak O., Höck V. and Delaloye M., 2002. The supra-subduction zone Pozantı-Karsantı ophiolite, southern Turkey: evidence for high-pressure crystal fractionation of ultramafic cumulates. Lithos, 65: 205-224.

Parlak O., Höck V., Kozlu H. and Delaloye M., 2004. Oceanic crust generation in an island arc tectonic setting, SE Anatolian Orogenic Belt (Turkey). Geol. Mag., 141: 583-603.

Parlak O., Karaoğlan F., Rızaoğlu T., Nurlu N., Bağcı U., Höck V., Önal Öztüfekçi A., Kürüm A. and Topak Y., 2013. Petrology of the İspendere (Malatya) ophiolite from the Southeast Anatolia: implications for the Late Mesozoic evolution of the southern Neotethyan Ocean. In: A.H.F. Robertson, O. Parlak and U.C. Ünlügenç (Eds.), Geological development of Anatolia and the easternmost Mediterranean Region. Geol. Soc. London Spec. Publ., 372: 219-247.

Parlak O., Rızaoğlu T., Bağcı U., Karaoğlan F. and Höck V., 2009. Tectonic significance of the geochemistry and petrology of ophiolites in southeast Anatolia, Turkey. Tectonophysics, 473: 173-187.

Parlak O., Yılmaz H. and Boztuğ D., 2006. Geochemistry and tectonic setting of the metamorphic sole rocks and isolated dykes from the Divriği ophiolite (Sivas, Turkey): evidence for melt generation within an asthenospheric window prior to ophiolite emplacement. Turk. J. Earth Sci., 15: 25-45.

Pearce J.A., 1982. Trace element characteristics of lavas from destructive plate boundaries. In: R.S. Thorpe (Ed.), Andesites. New York. John Wiley & Sons., p. 525-548.

Pearce J.A., 2003. Supra-subduction zone ophiolites: The search for modern analogues. In: Y. Dilek and S. Newcomb (Eds.), Ophiolite concept and the evolution of geological thought. Geol. Soc. Am. Spec. Pap., 373: 269-293.

Pearce J.A., 2008. Geochemical fingerprinting of oceanic basalts with applications to ophiolite classification and the search for Archean oceanic crust. Lithos, 100: 14-48.

Pearce J.A. and Norry M.J., 1979. Petrogenetic implications of Ti, Zr, Y, and Nb variations in volcanic rocks. Contrib. Miner. Petrol., 69: 33-47.

Pearce J.A., Lippard S.J. and Roberts S., 1984. Characteristics and tectonic significance of supra-subduction zone ophiolites. In: B.P. Kokelaar and M.F. Howells (Eds.), Marginal basin geology. Geol. Soc. London Spec. Publ., 16: 77-89.

Pearce J.A. and Robinson P.T., 2010. The Troodos ophiolitic complex probably formed in a subduction initiation, slab edge setting. Gondw. Res., 18: 60-81.

Perfit M.R., Gust D.A., Bence A.E., Arculus R.J. and Taylor S.R., 1980. Chemical characteristics of island-arc basalts: implications for mantle sources. Chem. Geol., 30: 227-256.

Perinçek D. and Kozlu H., 1984. Stratigraphical and structural relations of the units in the Afşin-Elbistan-Doğanşehir region (Eastern Taurus). In: O. Tekeli and M.C. Göncüoğlu (Eds.), Geology of the Taurus Belt. Proceed. Intern. Symp., MTA, Ankara, p. 181-198.

Pouchou J.L. and Pichoir F., 1984. A new model for quantitative X-ray microanalysis. Application to the analysis of homogeneous samples. Rech. Aerospat, 3: 13-38.

Putirka K.D., 2008. Thermometers and barometers for volcanic systems, In: K. D. Putirka and F. Tepley (Eds.), Rev. Miner. Geochem., 69: 61-120.

Rızaoğlu T., Bağcı U., Parlak O., Robertson A.H.F., Metin Y., Vergili Ö. and Booth M. 2010. Tectonic setting of ophiolitic rocks from the Hekimhan-Kuluncak (Malatya) region, Se Turkey. 7th Intern. Symp. Eastern Mediterranean Geology, October 2010 Adana, Abstr., p. 5.

Rızaoğlu T., Parlak O., Höck V. and İşler F., 2006. Nature and significance of Late Cretaceous ophiolitic rocks and its relation to the Baskil granitoid in Elazığ region, SE Turkey. In: A.H.F. Robertson and D. Mountrakis (Eds.), Tectonic development of the Eastern Mediterranean. Geol. Soc. London Spec. Publ., 260: 327-350.

Rızaoğlu T., Parlak O., İşler F., and Hoeck V., 2010. Geochemistry and tectonic significance of the cumulate rocks of the Kömürhen Ophiolite in Southeast Anatolia (Elazığ-Turkey). Proceed. Intern. Symp. Geology of Naturel Systems - Geolasi, Iasi - Romania, p. 35-37.

Robertson A.H.F., 2002. Overview of the genesis and emplacement of Mesozoic ophiolites in the Eastern Mediterranean Tethyan region. Lithos, 65: 1-67.

Robertson A.H.F. and Comas M., 1998. Collision-related processes in the Mediterranean region - Introduction. Tectonophysics, 298: 1-4.

Robertson A.H.F. and Dixon D.E., 1984. Introduction: aspects of the geological evolution of the Eastern Mediterranean. In: J.E. Dixon and A.H.F. Robertson (Eds.), The geological evolution of the Eastern Mediterranean. Geol. Soc. London Spec. Publ., 17: 1-74.

Robertson A.H.F., Parlak O., Metin Y., Vergili Ö., Taslı K., İnan N. and Soycan H. 2013. Late Palaeozoic-Cenozoic tectonic development of carbonate platform, margin and oceanic units in the Eastern Taurides, Turkey. In: A.H.F. Robertson, O. Parlak and U.C. Ünlügenç (Eds.), Geological development of Anatolia and the easternmost Mediterranean Region. Geol. Soc. London Spec. Publ., 372: 167-218.

Robertson A.H.F., Parlak O., Rızaoğlu T., Ünlügenç U.C., İnan N., Taslı K. and Ustaömer T., 2007. Tectonic evolution of the South Tethyan Ocean: Evidence from the Eastern Taurus Mountains (Elazığ region, SE Turkey). In: A.C. Ries, R.W.H. Butler and R.H. Graham (Eds.), Deformation of the continental crust. The Legacy of Mike Coward, Geol. Soc. London Spec. Publ., 272: 231-270.

Robertson A.H.F., Parlak O. and Ustaömer T., 2009. Melange genesis and ophiolite emplacement related to subduction of the northern margin of the Tauride-Anatolide continent, central and western Turkey. In: D.J.J. Van Hinsbergen, M.A. Edwards and R. Govers (Eds.), Collision and collapse at the Africa-Arabia-Eurasia subduction zone. Geol. Soc. London Spec. Publ., 311: 9-66.

Robertson A.H.F., Parlak O. and Ustaömer T., 2012. Overview of the Palaeozoic-Neogene evolution of Neotethys in the Eastern Mediterranean region (S Turkey, Cyprus, Syria). Petr. Geosci., 18: 381-404.

Robertson A.H.F., Ustaömer T., Parlak O., Ünlügenç U.C., Taslı K. and İnan N., 2006. The Berit transect of the Tauride thrust belt, S. Turkey: Late Cretaceous-Early Cenozoic accretionary/collisional processes related to closure of the southern Neotethys. J. Asian Earth Sci., 27: 108-145.

Saccani E. and Photiades A., 2004. Mid-ocean ridge and supra-subduction affinities in the Pindos Massif ophiolites (Greece): implications for magma genesis in a proto-forearc setting. Lithos, 73: 229-253.

Sarıfakıoğlu E., Özen H. and Winchester J.A., 2009. Whole rock and mineral chemistry of ultramafic-mafic cumulates from the Orhaneli (Bursa) ophiolite, NW Anatolia. Turk. J. Earth Sci., 18: 55-83.

Savostin L.A., Sibuet J.C., Zonenshain L.P., Le Pichon X. and Rolet J., 1986. Kinematic evolution of the Tethys belt, from the Atlantic to the Pamirs since the Triassic. Tectonophysics, 123: 1-35.

Şengör A.M.C. and Yılmaz Y., 1981. Tethyan evolution of Turkey: a plate tectonic approach. Tectonophysics, 75: 181-241.

Shervais J.W., 2001. Birth, death and resurrection: the life cycle of suprasubduction zone ophiolites. Geochem. Geophys. Geosyst., 2 (1): 1-45.

Sisson T.W. and Grove T.L., 1993. Experimental investigations of the role of H_2O in calc-alkaline differentiation and subduction zone magmatism. Contrib. Miner. Petrol., 113: 143-166.

Smith J.V. and Brown W.L., 1988. Feldspar minerals, 1. Crystal structures, physical, chemical and mineralogical properties. Springer-Verlag, Berlin, Heidelberg, New York, 828 pp.

Spandler C., Hermann J., Arculus R., and Mavrogenes J., 2003. Redistribution of trace elements during prograde metamorphism from lawsonite blueschist to eclogite facies: Implications for deep subduction-zone processes. Contrib. Miner. Petrol., 146: 205-222.

Stern R.J., 1979. On the origin of andesite in the northern Mariana island arc: implications for agrigan. Contrib. Miner. Petrol., 68: 207-219.

Sun S.S. and Mcdonough W.F., 1989. Chemical and isotopic systematics of ocean basalts: Implications for mantle composition and processes. In: A.D. Saunders and M.J. Norry (Eds.), Magmatism in the ocean basins. Geol. Soc. London Spec. Publ., 42: 313-346.

Takagi D., Sato H. and Nakagawa M., 2005. Experimental study of a low-alkali tholeiite at 1-5 kbar: optimal condition for the crystallization of high-An plagioclase in hydrous arc tholeiite. Contrib. Miner. Petrol., 149: 527-540.

Tanırlı M. and Rızaoğlu T., 2016. Whole-rock and mineral chemistry of mafic cumulates from the low-Ti ophiolite in the southern part of Kahramanmaraş, Turkey. Russian Geol. and Geophys., 57(10): 1398-1418.

Taylor W.R., 1998. An experimental test of some geothennometer and geobarometer formulations for upper mantle peridotites with application to the thermobarometry of fertile lherzolites and garnet websterite. N. Jb. Miner. Abh., 172: 381-408.
Thy P., 1987. Magmas and magma chamber evolution, Troodos ophiolite, Cyprus. Geology, 15: 316-319.
Thy P., 1990. Cryptic variation of a cumulate sequence from the Plutınic Complex of the Troodos Ophiolite. In: J. Malpas, E. Moores, A. Panayiotou and C. Xenophontos (Eds.), Ophiolites, oceanic crustal analogues. Proceed. Troodos Ophiolite Symp., p. 165-172.
Thy P., Schiffman P. and Moores E.M., 1989. Igneous mineral stratigraphy and chemistry of the Cyprus Crustal Study Project drill core in the plutonic sequences of the Troodos Ophiolite. Geol. Surv. Can. Paper, 88 (9): 147-185.
Tiepolo M. and Tribuzio R., 2005. Slab-melting during Alpine orogeny: evidence from mafic cumulates of the Adamello batholith (Central Alps, Italy). Chem. Geol., 216: 271-288.
Tribuzio R., Tiepolo M. and Thirlwall M.F., 2000. Origin of titanian pargasite in gabbroic rocks from the Northern Apennine ophiolites (Italy): insights into the late-magmatic evolution of a MOR-type intrusive sequence. Earth Planet Sci. Lett., 176: 281-293.
Wager L.R., Brown G.M. and Wadsworth W.J., 1960. Types of igneous cumulates. J. Petrol., 1: 73-85.
Wallin E.T. and Metcalfe R.V., 1998. Supra-subduction zone ophiolite formed in an extensional forearc: Trinity Terrane, Klamath Mountains, California. J. Geol., 106: 591-608.
Whitney D.L. and Evans B.W., 2010. Abbreviations for names of rock-forming minerals. Am. Miner., 95: 185-187.
Yalçin H., Gündoğdu M.N., Gourgaud A., Vidal P. and Uçurum A., 1998. Geochemical characteristics of Yamadağı volcanics in central east Anatolia: an example from collision-zone volcanism. J. Volcan. Geotherm. Res., 85: 303-326.
Yalınız K.M. and Göncüoğlu M.C., 1999. Clinopyroxene compositions of the isotropic gabbro from the Sarıkaraman Ophiolite: New evidence on supra-subduction zone type magma genesis in Central Anatolia. Turk. J. Earth Sci., 8: 103-111.
Yalınız K.M., Floyd P. and Göncüoğlu M.C. 1996. Supra-subduction zone ophiolites of Central Anatolia: geochemical evidence from the Sarikaraman ophiolite, Aksaray, Turkey. Miner. Mag., 60: 697-710.
Yılmaz H., Dumanlılar Ö., Ay Y. and Yılmaz A., 2005. Tectonostratigraphic characteristics of ophiolitic rocks in the Hekimhan-Kuluncak (Malatya) region. 58th Turk. Geol Symp., Proceed., p. 271 (in Turkish with English abstract).
Yoder H.S., 1969. Calc-alkaline andesites: experimental data bearing the origin of assumed characteristics. In: A.R. McBirney (Ed.), Proceed. Andesite Conference. Oreg. Dept. Geol. Mineral. Ind. Bull., 65: 43-64.
Yogodzinski G.M., Rubenstone J.L., Kay S.M. and Kay R.W., 1993. Magmatic and tectonic development of the western Aleutians: An oceanic arc in a strike-slip setting. J. Geophys. Res.., 98: 11807-11834.

Received, January 2, 2017
Accepted, May 12, 2017